NANO · MICRO small
www.small-journal.com

Influence of Impurities from Manufacturing Process on the Toxicity Profile of Boron Nitride Nanotubes

*Vamsi Kodali, Keun Su Kim, Jenny R. Roberts, Lauren Bowers, Michael G. Wolfarth, John Hubczak, Xing Xin, Tracy Eye, Sherri Friend, Aleksandr B. Stefaniak, Stephen S. Leonard, Michael Jakubinek, and Aaron Erdely**

The toxicity of boron nitride nanotubes (BNNTs) has been the subject of conflicting reports, likely due to differences in the residuals and impurities that can make up to 30–60% of the material produced based on the manufacturing processes and purification employed. Four BNNTs manufactured by induction thermal plasma process with a gradient of BNNT purity levels achieved through sequential gas purification, water and solvent washing, allowed assessing the influence of these residuals/impurities on the toxicity profile of BNNTs. Extensive characterization including infrared and X-ray spectroscopy, thermogravimetric analysis, size, charge, surface area, and density captured the alteration in physicochemical properties as the material went through sequential purification. The material from each step is screened using acellular and in vitro assays for evaluating general toxicity, mechanisms of toxicity, and macrophage function. As the material increased in purity, there are more high-aspect-ratio particulates and a corresponding distinct increase in cytotoxicity, nuclear factor-κB transcription, and inflammasome activation. There is no alteration in macrophage function after BNNT exposure with all purity grades. The cytotoxicity and mechanism of screening clustered with the purity grade of BNNTs, illustrating that greater purity of BNNT corresponds to greater toxicity.

1. Introduction

Boron nitride nanotubes (BNNTs) have structural similarity to carbon nanotubes (CNTs) but have several advantages including a wider band gap, optical transparency, radiation shielding, and higher thermal and chemical stability. The applications for BNNTs include use as structural reinforcements in composites, radiation shielding, thermal management, energy harvesting, and biomedicine.[1,2] BNNTs, like their CNT counterparts, are not identical and have heterogeneous physico-chemical characteristics and residuals that are primarily driven by the manufacturing and purification processes utilized. BNNTs have been synthesized by various methods including arc discharge, ball milling, chemical vapor deposition (CVD), template assisted synthesis, laser ablation, and thermal plasma jet methods.[3–6] Within these broad classification of manufacturing approaches, BNNTs can be prepared via a myriad of alterations in process conditions, precursors, and catalyst use. These multitude of approaches result in generation of varied BNNTs in terms of physico–chemical characteristics including length, diameter, number of concentric layers, impurities, and leftover residuals. Some of the major impurities and residuals reported in BNNT materials include boron allotropes, boron oxide, turbostratic boron nitride (BN), varying forms of BN impurities including unstacked hexagonal boron nitride (hBN), BN flakes, BN shells, crystalline hBN, intermediate particulate like hBN-encapsulated boron particulate, and other B—N—H compounds

V. Kodali, J. R. Roberts, M. G. Wolfarth, J. Hubczak, X. Xin, T. Eye, S. Friend, S. S. Leonard, A. Erdely
Health Effects Laboratory Division
National Institute for Occupational Safety and Health
Morgantown, WV 26505, USA
E-mail: efi4@cdc.gov

V. Kodali, A. Erdely
Department of Physiology and Pharmacology
School of Medicine
West Virginia University
Morgantown, WV 26506, USA

The ORCID identification number(s) for the author(s) of this article can be found under https://doi.org/10.1002/smll.202203259.

K. S. Kim, M. Jakubinek
Division of Emerging Technologies
National Research Council Canada
100 Sussex Drive, Ottawa, ON K1A 0R6, Canada

L. Bowers, A. B. Stefaniak
Respiratory Health Division
National Institute for Occupational Safety and Health
Morgantown, WV 26505, USA

S. S. Leonard
Department of Pharmaceutical Science
School of Pharmacy
West Virginia University
Morgantown, WV 26506, USA

DOI: 10.1002/smll.202203259

such as ammonia borane.[7–13] Depending on the manufacturing method employed, other metal catalyst residuals like iron and nickel were also present.[14,15] Morphologically, apart from the tubular structures of BNNT, the impurities appear as a combination of fibrous, sheet- and powder-like structures. Based on the synthesis route and the impurity/residual targeted for removal, several purification strategies have been proposed including gas phase purification by chlorine etching,[16] acid washing,[17] hydrocarbon solvent processing,[18] wet thermal etching,[19] hot-water washing,[17] surfactant wrapping and centrifugation,[10,20] gel column chromatography,[21] and sonication assisted filtration.[10]

With a wide range of applications and progress in development of efficient large-scale production processes,[22–25] the next step in successful large-scale commercialization is to determine if these tubes cause any adverse pulmonary toxicity, as inhalation is a prominent route of exposure in occupational settings. Although BN is chemically stable and relatively inert, properties of BNNT including aspect ratio, oxidant-producing impurities, defects in the material, and alteration in total dose of exposure due to impurities with varying densities can influence the toxicity response of the material, similar to other high aspect ratio engineered nanomaterials. Previous studies evaluating toxicity were performed using BNNTs produced from different manufacturing processes having varying purity grades and impurities. Some of these studies include high-temperature high-pressure process,[26,27] hydrogen assisted induction thermal plasma process using pure hexagonal boron nitride powder as feedstock (hydrogen-assisted BNNT synthesis [HABS]),[28] CVD,[29,30] and ball milling/annealing method.[31–34] With these variations, it is not surprising to observe an inconsistency in the reported toxicity profile among these investigations, though some consensus can be drawn from more than decade old research in this area. The toxicity of BNNT correlated with length.[28,30] The toxicity induced was dependent on biocompatible coating and dispersion procedure (sonication) as they had an influence on dimension and agglomeration. Apart from dose and exposure time, toxicity of BNNT in vitro was also found to be dependent on cell model used[29] for testing. Macrophages had the greatest response while kidney cell line had the least, this may be due to differences in uptake capacity of these cells.

Our previous toxicity evaluation using a 50% BNNT mixture[26,27] showed good correlation in the toxicity response to BNNT between in vitro (THP-1 macrophages) and in vivo (C57BL/6J mice) models. BNNTs, like other high aspect ratio materials, caused acute lung damage and inflammation by inducing cytotoxicity, oxidative stress, inflammation, and inflammasome activation. In vivo, only the high dose of BNNT (40 μg/mouse) induced acute lung injury and inflammation, whereas the low dose (4 μg/mouse) did not. The responses were observed as early as 4 h post exposure and peaked at 7 days but resolved over time. The exposure did not progress to pathological conditions like fibrosis or alterations in the lungs.

The mechanism of toxicity points to shape or aspect ratio of the material being a major influence as lysosomal damage and a marked increase in inflammasome activation was observed with these exposures. The role of oxidant-generating residual/impurities contributing toward acute toxicity, oxidative stress, and inflammation was not investigated. In the current work, we evaluated the toxicity of BNNT produced by HABS and the effect of varying proportions of BNNT to residuals/impurities after each stage of the systemic purification process on the toxicity profile. The as-produced BNNTs (AP-BNNT) were produced using HABS and were purified to remove elemental boron using a gas phase purification (boron removed, BR-BNNT). The BR-BNNT samples were further purified by sequential water and acetone washing followed by filtration to dissolve soluble residuals/impurities and remove low aspect ratio particulate (washed, W1- and W2-BNNT). The precursor, hBN, was used as a control for the toxicity studies. Extensive characterization was performed including Brunauer, Emmett, and Teller surface area (BET surface area), tapping density, Fourier transform infrared spectroscopy (FTIR), X-ray photoelectron spectroscopy (XPS), scanning electron microscopy (SEM) with energy dispersive X-ray spectroscopy (EDX), thermogravimetric analysis (TGA), and hydrodynamic sizing by light scattering (dynamic light scattering [DLS]) to relate the toxicity response to the material characteristics. THP-1 macrophages were used for screening and challenged with the varying purity materials. The responses screened included cytotoxicity, membrane damage, alteration in inflammatory cytokine/chemokine production, alteration in macrophage function, and prominent molecular mechanisms of pulmonary toxicity induced by similar classes of materials including inflammasome and nuclear factor-κB (NF-κB) activation. The various toxicity responses were clustered to determine the influence of purity grade on the toxicity outcome.

2. Results and Discussion

2.1. Purification and Physico–Chemical Characterization

The main features of the FTIR spectra (**Figure 1**A) showed absorptions around 780 cm^{-1} and just below 1350 cm^{-1}, which are characteristics of B—N bonding in hBN and BNNTs. These features are dominant for all samples but most distinct for the solvent-washed BNNTs (W1- and W2-BNNT). In contrast, AP- and BR-BNNT samples show more absorption in the N—H region around 3200 cm^{-1} and additional features in the 900–1100 cm^{-1} range, which are attributed to hBN impurities.[23] These additional features are largely absent after solvent washing and lead to a flatter absorption in the N—H region.

FTIR spectra of species desorbed from the BNNT materials during heating were obtained from coupled thermogravimetric analysis with Fourier transform infrared spectroscopy (TGA-FTIR) (Figure 1B), which indicates desorption of ammonia and water during heating in argon. The TGA in air (Figure S1, Supporting Information) shows a significant mass increase for AP-BNNTs above 600 °C. This is consistent with the known boron impurity, which also causes the brown color of this material (Figure S2, Supporting Information) and is converted to boron oxide resulting in a white sample after TGA. Other samples show mass increase only above ≈900 °C. This is attributed to oxidation of materials with dangling bonds or defective sites, and is not observed when the temperature and time for this gas-phase purification process are increased.[16] Samples purified by washing show more oxidation above 900 °C, relative to the BR-BNNT material, which could be associated with defects

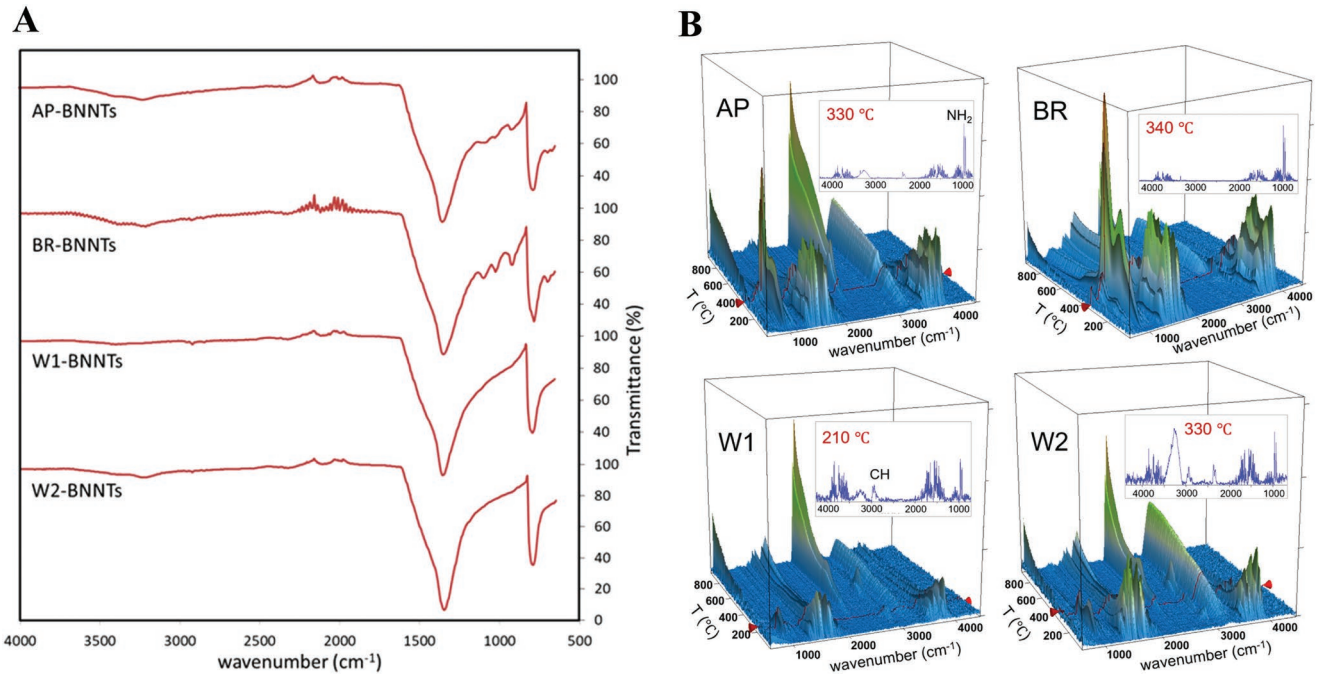

Figure 1. A) Comparison of attenuated total reflection Fourier transform infrared spectroscopy (ATR-FTIR) spectra of as-produced BNNTs with BNNTs from various sequential purification steps including gas-phase chlorine etching and water/solvent washing. B) Thermogravimetric analysis coupled to Fourier transform infrared spectroscopy (TGA-FTIR) data of various purity grade BNNTs showing FTIR absorption spectra of desorbed species as a function of temperature during TGA heating under argon.

created due to sonication. TGA in argon (Figure S1, Supporting Information) shows that all materials differ mainly in the amount of mass loss at lower temperatures, which is attributed primarily to adsorbed water and ammonia seen in the coupled FTIR measurements (Figure 1B). Ammonia is a by-product in the BNNT synthesis by HABS and its characteristic double-peak, observed just below 1000 cm^{-1}, is less prominent and not observed at lower temperature for the solvent-washed materials. A mass loss slightly above 400 °C for solvent washed samples is associated with a CH absorption and was subsequently attributed to unintended polymer contamination from plastic spray bottles used in the washing.

SEM images verify the increase in purity (the relative amount of high-aspect ratio, BNNT-like and BNNT-bundle-like features) from AP- to BR- to W1/W2-BNNTs (**Figure 2**), indicated by observation of fewer low-aspect-ratio features. SEM analysis of 200 particulate of the highest purity BNNT (W2) showed that BNNT had a geometric mean length (geometric standard deviation [GSD]) of 1.68 µm (1.9) and a geometric mean diameter (GSD) of 0.017 µm (1.33). The arithmetic mean length and diameter was 2.095 ± 1.6 µm and 0.019 ± 0.005 µm, respectively. The diameter of the agglomerates in dispersion medium had a geometric mean (GSD) of 0.59 µm (2.49). Compositional analysis from SEM-EDX (**Table 1**) shows the imaged material contains primarily boron and nitrogen and that the boron content is reduced substantially for BR-BNNT in comparison to AP-BNNT. This is to be expected after the purification process to react and remove elemental boron impurities. Carbon, which is attributed primarily to contamination during sample preparation (SEM-EDX samples were produced by dispersion and filtration to form a sheet, which was mounted on carbon tape), and oxygen is relatively consistent and does not show a trend across the samples. The elemental compositions are not changed by the solvent washing since the impurities removed are also expected to be BN materials. A chlorine peak was observed in EDX (**Figure 3**A) and was added to the analysis after fixing the B and N results to allow consistent fitting of overlapping peaks. This analysis indicates a low content of chlorine (<0.2 at%) despite the use of chlorine in the boron removal process, validating that it is removed as a gaseous product (e.g., BCL_3). Cl content does increase from 0.02 at% in AP-BNNTs, which are not expected to contain any chlorine, to 0.12 at% following boron-removal but is detected only at 0.2 and 0.07 at% in the highest purity (W1- and W2-BNNT respectively).

Notably, there was no significant indication of chlorine in the XPS spectra of purified samples. The Cl 2p peak overlaps with the boron region; however, XPS peaks are not observed for the Cl 2s (270 eV) or the LLM Auger line (1306 eV), suggesting that the potential chlorine remaining in any sample is at or below the detection limit. High-resolution spectra (Figure 3B) show that the peak associated with elemental boron (near 188 eV) disappears following the gas-phase purification (BR-BNNTs). The high binding-energy shoulder associated with the presence of B—O in the vicinity of ≈192 eV also decreased with purification. Fitting the component peaks in the B 1s region (Figure 3C) indicates that the boron environment becomes more BN-like with increasing purification.[35] In order to obtain consistent fitting results for the B1s spectra, the component peaks were constrained based on the fitting results for the AP-BNNT sample, where peaks associated with three chemical environments (B—N, B—O, and B—B) are most clear. The larger width for the B—O component peak indicates that environment is

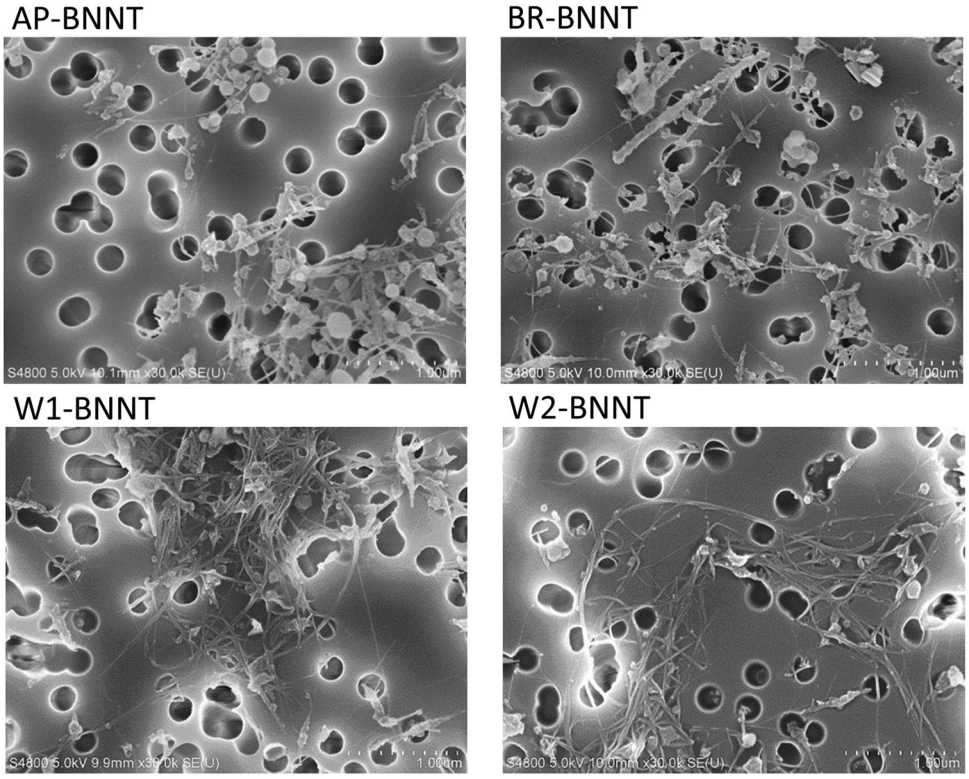

Figure 2. Scanning electron microscopy (SEM) images of various purity grade BNNTs. A decrease in the number of low aspect ratio and an increase in high aspect ratio particulate can be observed as the material goes through sequential purification process.

more variable (encompasses components including N—B—O and O—B—O), in comparison to the more intense and narrower B—N peak. While the quantitative fitting results are significantly affected by the fitting assumptions, the XPS verifies, independent of the specific fitting approach, both the removal of elemental boron for BR-BNNTs and that the subsequent washing increases the BN content/quality of the material.

The various BNNT purity forms and hBN were tested for endotoxin contamination by limulus amebocyte lysate assay and had endotoxin below the lower detection limit (<0.12 EU mL^{-1}).

BNNT materials are truly a mixture consisting of particulates of various morphologies including sphere-like flakes and tubes. As such, surface area and density of the material can be a good qualitative representation of the materials characteristic. Also, surface area has been shown to be an important parameter that correlates with toxicity of certain nanomaterials.[36,37] On an equal mass to mass comparison, with increasing purity there was an increase in surface area. Surface area of hBN, AP, BR, W1, and W2 is 23.6, 70.7, 103.3, 150.7, and 144.9 m^2 g^{-1}, respectively (**Table 2**). Surface area of the pure form W1-BNNT was twofold that of AP-BNNT and sixfold compared to that of hBN. Surface area had a direct correlation (Spearman's $\rho = 1$, $p < 0.001$) to purity (XPS %BN). The surface areas of all the BNNTs evaluated in the current work were lower than the surface area of BNNT-M (183 m^2 g^{-1}) that was produced using a high-temperature high pressure process,[25] the in vitro and in vivo pulmonary toxicity of which has been evaluated by us previously.[26,27] Density of the material can influence toxicity by influencing the kinetics and dynamics of dose through settling velocity in submerged cell culture models and aerodynamic behavior in inhalation exposures.[38] Also, most exposures are evaluated on a mass basis and density being directly proportional to mass, can influence the particulate number during the exposures and consequently toxicity response for some nanomaterials. The tapping densities of hBN, AP, BR, and W1 were 278.7, 20.2, 20.1, and 30.4 mg cm^{-3}, respectively (Table 2). There was more than tenfold decrease in density as the material transformed from hBN to AP-BNNT. There was no change

Table 1. Compositional analysis (atomic%) of BNNT materials using SEM-EDX. With the exception of chlorine, other elements detected at <1% (Al, Na, Mg, Ca, and Si) in the EDX measurement were excluded from the analysis.

	B	N	C	O	Cl
AP-BNNT	46 ± 4	34 ± 2	15 ± 4	4.9 ± 0.8	0.02 ± 0.01
BR-BNNT	37 ± 2	43 ± 2	14 ± 3	5.6 ± 0.5	0.12 ± 0.04
W1-BNNT	39.3 ± 0.6	46.3 ± 0.1	10.4 ± 0.6	3.8 ± 0.03	0.2 ± 0.03
W2-BNNT	35.8 ± 0.3	43.1 ± 0.6	16.2 ± 0.6	4.9 ± 0.2	0.07 ± 0.004

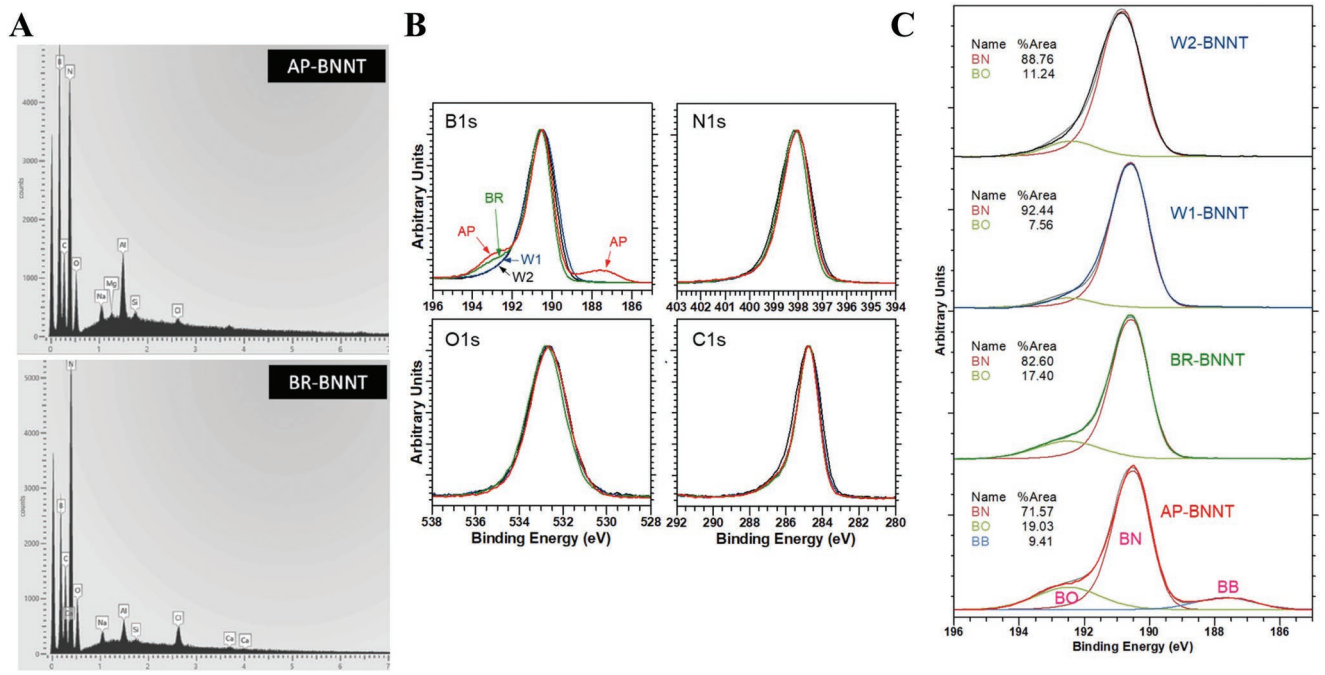

Figure 3. A) SEM-EDX showing peaks at energies (eV) assigned to B, N, O, and C as well as other elements present at <1 at%. Chlorine, used in the boron-removal step, is observed more clearly for BR-BNNTs (0.12 at%) relative to AP-BNNTs (0.02 at%). B) High resolution XPS spectra in the B1s, N1s, C1s, and O1s regions for AP- (red), BR- (green), and W- (blue). C) Component fitting for the B1s region for (top to bottom): W2-, W1-, BR-, and AP-BNNT.

in densities of AP- and BR-BNNTs, but as the material went through wash cycles to washed BNNT (W-BNNT) there was an ≈33% increase in density. BNNT-M produced using a high-temperature high-pressure process had a density similar in range to W-BNNTs, the highest purity of BNNT material evaluated in the current study.

The hydrodynamic diameter, a qualitative reflection of the agglomeration state of the BNNT material in cell culture media, ranged between 280 and 400 nm for hBN and BNNTs of various purity grades (Table 2). The AP-BNNT had the smallest hydrodynamic diameter. hBN had the lowest while purified W-BNNTs had the highest polydispersity. This increase can be potentially attributed to the presence of higher aspect ratio particulate with increasing BNNT purity. Zeta potential (ζ) of the particulate, the charge on the nanomaterial surface in an aqueous media, was evaluated by measuring electrophoretic mobility of the particles in cell culture media by phase analysis light scattering. Zeta potential can define the agglomeration behavior and toxicity induced by the particulate. There was minimal discrepancy in Zeta potential between various BNNTs in cell culture media (Table 2). This could be attributed to strong Debye screening by the ions present in the cell culture media.

2.2. Acellular Oxidative Stress Potential

Oxidative stress has been associated with various toxicological endpoints and is considered as a predictive paradigm for toxicity induced by nanomaterials. Oxidative stress is generated through several direct and indirect mechanisms.[39] Acellular reactive oxygen species (ROS) measured by electron paramagnetic resonance (EPR) has been found to be a good predictor of nanomaterial toxicity, especially with nanomaterial that can generate ROS directly.[40,41] High-aspect-ratio materials like CNTs and BNNTs can induce ROS in cells through indirect mechanism which include perturbing various cellular signaling

Table 2. BNNT materials employed.

Name	Gas-phase purification	Number of wash cycles		Powder production/ homogenization	BET surface area [$m^2\ g^{-1}$]	Density [mg cm^{-3}]	Hydrodynamic Diameter [nm]	Zeta Potential [mV]
		[water]	[acetone]					
Hexagonal boron nitride (hBN)	No	N/A	N/A	—	23.64 ± 0.05	278.7	350.8 ± 7.9	−12.7 ± 1.2
AP-BNNT[23]	No	N/A	N/A	Grinding	70.7 ± 0.34	20.2	284.8 ± 31.3	−12.7 ± 1.1
BR-BNNT[16]	Yes	N/A	N/A	Grinding	103.3 ± 0.36	20.1	343.9 ± 98	−12.1 ± 0.9
W1-BNNT	Yes	2	4	Freeze-drying	150.67 ± 0.25	30.4	396.2 ± 66	−12.1 ± 0.9
W2-BNNT	Yes	2	8	Freeze-drying	144.9 ± 0.19	ND	354.3 ± 24	−11.4 ± 1.7

processes,[26,42] but even high aspect ratio material can induce direct ROS generation due to the presence of metal residuals, oxidative impurities, and surface defects.[43–45]

Reactivity or acellular oxidative stress potential of BNNT as it went through various stages of purification was assessed using EPR with spin trapping. Spin trapping involves the addition reaction of a short-lived radical with a paramagnetic compound (i.e., spin trap) to form a relatively long-lived free radical product, termed the spin adduct, which can be studied with the conventional EPR. Using the spin trap agent, 5,5-dimethyl-1-pyrroline-N-oxide (DMPO), the ability of the various BNNT materials and hBN to generate OH· radicals was detected after reacting with H_2O_2. The 1:2:2:1 spectra (**Figure 4**A), a characteristic of the OH· radical, showed a marked difference between the 2 mM Cr (VI) positive control and the BN samples. Quantification (Figure 4B) of the signal intensity (peak height) shows that there was approximately threefold change between BN samples and Cr (VI). There was a statistically significant change between all the test groups compared to the positive control sample Cr (VI) and negative control sample (DMPO with no H_2O_2). Within the BN samples, hBN was the most reactive, producing the greatest amount of OH· radicals followed by AP-BNNT, BR-BNNT, W1-, and W2-BNNTs, respectively. On an equal mass basis, surface reactivity or oxidant production generally trends positively with surface area of the nanomaterial.[46] There was a negative correlation ($R^2 = 0.96$, $p = 0.004$; Spearman's $\rho = -0.9$, $p = 0.04$) between surface area of the various materials and the amount of radicals produced (Figure S3, Supporting Information), suggesting additional components like impurities/residuals in the material were stimulating the oxidant production.

Although the absolute magnitude decreased with increasing purity, analysis of the variance showed that there was no significant alteration in the generated radicals between BR, W1-, and W2-BNNTs. Significant OH· radicals were produced by hBN and AP-BNNT compared to the purer BNNTs. Boron and especially BN materials are fairly stable and are not remarkably reactive. Residuals, impurities, and structural changes inherent (from raw material) or induced during the extreme conditions of the manufacturing process, could alter the reactivity of the BN material.[47–49] High resolution XPS spectra of B 1s, N 1s, O 1s, and C 1s showed that, with changing purity, there was no change in the total surface oxygen as evident from the O 1 spectra (Figure 3B) but a closer analysis of B 1 spectra by peak fitting (Figure 3C) showed a B—O peak. This peak decreased with increasing purity and directly correlated with oxidant production. Other boron impurities were also present in the AP-BNNT as evident from B—B peak. TGA analysis (Figure 3C) further confirmed AP-BNNT had defects and oxidative impurities. Finally, B—N peak (XPS %BN), a representation of BN purity increased with the purification steps, and this was inversely proportional to the oxidant production ($R^2 = 0.998$, $p = 0.03$, Spearman's $\rho = -1$, $p < 0.0001$).

Taken together, there was a significant production of radicals associated with hBN and AP-BNNT and not a significant difference after the gas purification. It is surprising to see hBN showing this level of reactivity; one potential reason for hBN reactivity could be due to presence of impurities and defects. On the other hand, AP-BNNT inducing significant radical production is not surprising, owing to the presence of various impurities and residuals. Gas phase purification, removing the boron impurities effectively, reduced many of these oxidant generating components and the trend in decreasing reactivity with the sequential water and acetone washing suggests more wash steps could potentially reduce the level of oxidants further, and the pure high-aspect-ratio BNNT structures were likely not the reactive or radical producing component in the BNNT mixtures.

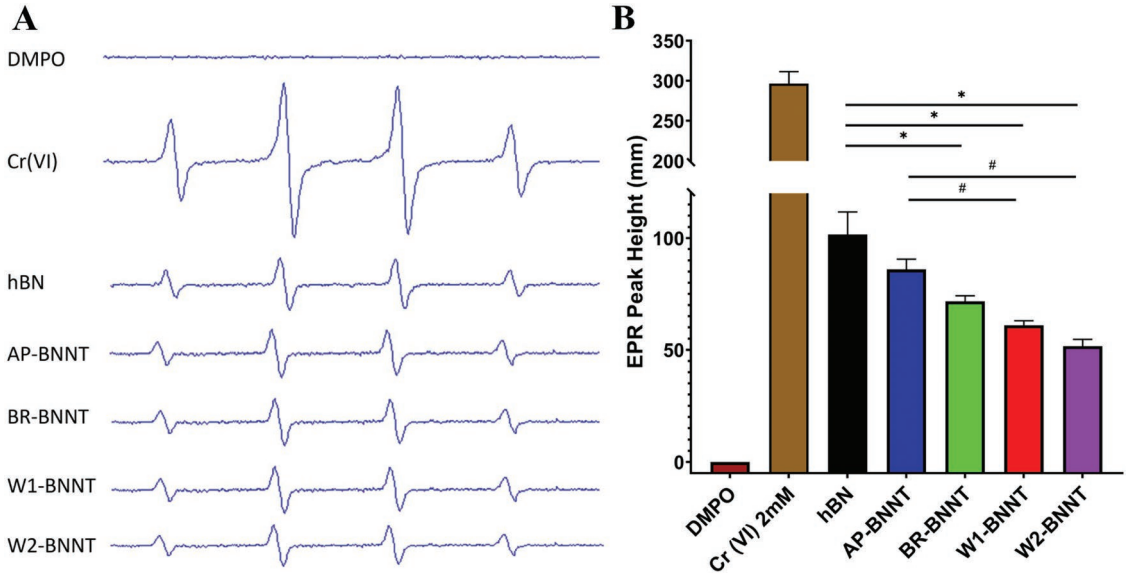

Figure 4. A) Representative electron paramagnetic resonance spectroscopy (EPR) spectra and B) EPR peak height with negative control (DMPO only), positive control (Cr (VI)), hBN, and various purity grade BNNTs AP, BR, W1, and W2. Data analyzed by one way ANOVA showed hBN and all purity grade BNNTs had a significant change ($p < 0.05$) compared to positive or negative control. Within the test group, hBN (*) and AP-BNNT (#) induced significant ($p < 0.05$) free radicals compared to other BNNTs.

2.3. Cytotoxicity and Membrane Damage

The effect of purity on the ability of BNNTs to induce cytotoxicity and membrane damage was evaluated by measuring the macrophage's ability to metabolize the cell proliferation reagent WST-1 and lactate dehydrogenase (LDH) released relative to the total LDH in the cells. These parameters were evaluated in differentiated THP-1 macrophages over a wide dose range 0–100 μg mL^{-1} after 24 h of exposure. Previously we found THP-1 macrophages had a comparable response to an in vivo acute toxicity response.[26,27] The four purity grades of BNNTs and hBN induced a dose-dependency in cytotoxicity. W1- and W2-BNNTs, the highest purity BNNTs (XPS %BN) and the material having the highest amount of high aspect ratio material, had a marked difference in the cytotoxic dose response compared to the other materials (**Figure 5**A). At the highest concentration the viability reduced by ≈40%. This is in line with a previous study using HABS-prepared BNNTs with some comparable purification steps, where a size-dependent cytotoxicity was reported in cardiomyocytes.[28] BNNTs dispersed and purified using an alternative approach decreased cytotoxicity in fibroblast (3T3-L1) and epithelial cells (CHO-K1).[50] Size, surface coating (used for dispersion), and remaining impurities could be the reason for the difference in the observed response. The increase in toxicity was further confirmed by evaluating the active form of caspase 3/7 as a marker for apoptosis (Figure S4, Supporting Information). As seen with the other toxicity measures, a dose-dependent increase in caspase 3/7 was observed with the purified BNNT (W2-BNNT) but not with hBN. Particle internalization in the cells was confirmed by TEM (Figure S5, Supporting Information).

Segmentation of the dose-response using Ward distance-based hierarchical clustering (HCA)[51] confirmed the observed difference between the groups (Figure 5B). There are broadly two clusters in the treatment groups. hBN and AP-BNNT formed the first cluster while the purified BNNTs, BR-BNNT, W1-, and W2-BNNT formed the second. Within the second cluster, W1- and W2-BNNT formed a cluster. Across the dose-response, broadly there were two clusters, the first response across doses 50 and 100 μg mL^{-1} and the second response across lower doses. Within this second cluster the response from 6.25, 12.5, and 25 μg mL^{-1} separated from further lower dose exposures.

The benchmark dose (BMD) for the dose responses were 36.66, 39.47, 65.88, 17.25, and 17.24 μg mL^{-1} for hBN, AP-BNNT, BR-BNNT, W1-BNNT, and W2-BNNT, respectively (Figure 5D). The BMD:BMDL ratio, a measure of reliability or uncertainty in the BMD model, showed the models to be a good fit to the

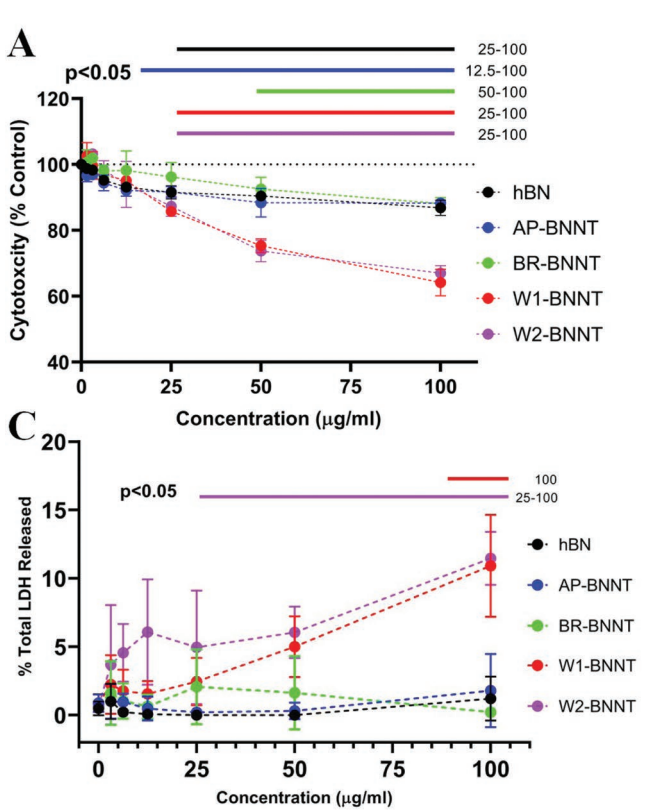

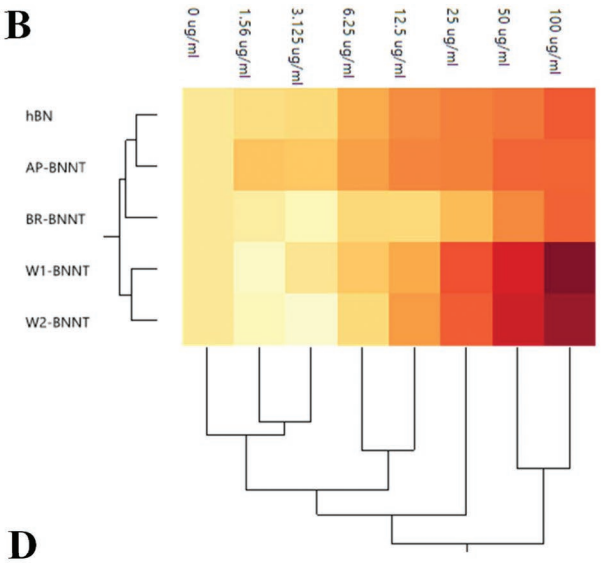

D

	BMD	BMDL	BMDU	BMD/BMDL
hBN	36.66 μg/ml	29.89 μg/ml	46.5 μg/ml	1.2
AP-BNNT	39.47 μg/ml	23.72 μg/ml	84.5 μg/ml	1.7
BR-BNNT	65.88 μg/ml	49.83 μg/ml	88 μg/ml	1.3
W1-BNNT	17.25 μg/ml	14.5 μg/ml	20 μg/ml	1.2
W2-BNNT	17.24 μg/ml	14.74 μg/ml	19.8 μg/ml	1.2

Figure 5. A) Cytotoxicity measured by evaluating the change in WST-1 metabolism in macrophages exposed to 0–100 μg mL^{-1} of either hBN or various purity grade BNNTs AP, BR, W1, and W2. B) Hierarchal clustergram of the cytotoxic response showing grouping of the material based on their response. C) Dose-response in membrane damage induced due to exposure of hBN or various purity grade BNNTs for 24 h at 0–100 μg mL^{-1}. D) Benchmark dose (BMD), the lower (BMDL), and higher limit (BMDU) based on the cytotoxicity response. Model selection for BMD was performed based on the lowest Akaike Information Criterion (AIC). The bars above the charts represent significant response ($p < 0.05$) from control cells with no exposure determined by two-way ANOVA analysis followed by pairwise comparison using Tukey's multiple comparisons test.

measured dose-response relationship. The BMD dose of BR-BNNT was the highest and was greater than hBN or AP-BNNT, suggesting boron removal reduced the toxicity of the BNNT materials. This could be due to the oxidants present in hBN and AP-BNNT. There was higher heterogeneity in the dose response of AP- and BR-BNNTs, while hBN, W1, and W2 had lower heterogeneity. The lower toxicity observed in hBN and AP-BNNT could be due to the presence of various impurities that masked the aggregate toxicity and due to presence of lower high-aspect-ratio particulates. Furthermore, the higher BMD, that is, lower toxicity of BR-BNNT (gas purified BNNTs), suggests that the impurities and residuals in hBN and AP-BNNT may have a mixed toxicity response where some components possibly induce toxicity by causing an increase in oxidant radical production while the other components ameliorate the response. LDH release was used to evaluate membrane damage due to exposure of various BNNTs and hBN (Figure 5C). Compared to control cells, exposure to 0–100 μg mL^{-1} of hBN, AP-, and BR-BNNT showed no statistical difference in the degree of membrane damage. W1-BNNT caused significant membrane damage at the highest concentration and W2-BNNT caused membrane damage from 25 to 100 μg mL^{-1}. The magnitude in LDH response of W1- and W2-BNNTs was similar to or slightly lower than levels previously observed with BNNT-M.[26] The change in cellular metabolism was much more sensitive to BNNT exposure than LDH release. Although the effect size of these two responses varied, both assays showed similar segregation in the test groups. The aggregate of these two responses showed hBN, AP-, and BR-BNNTs formed a cluster while W1 and W2, the highest-grade purity BNNTs, clustered together. This clustering in the toxicity response could be attributed to increasing high-aspect-ratio particulates with increasing purity of the BNNTs.

2.4. Mechanism-Based Screening

Mechanistic studies investigating acute toxicity response to various environmental and occupational exposures consisting of spherical, 2D, or high aspect ratio particulates highlight the role of molecular initiating events NF-κB and NLRP3 inflammasome activation.[52–57] The influence of impurities and increase in presence of high aspect ratio particulate with increasing BNNT purity was further investigated using a mechanism-based screening approach. This approach evaluated the dose response in activation of these molecular initiating events with hBN, AP-, BR-, W1-, and W2-BNNTs. The effect of screening was quantified using the Toxicological Prioritization Index (ToxPi) framework.

2.4.1. Nuclear Factor-κB Activation

As a homeostatic response to pulmonary particulate exposure, the body elicits an inflammatory response to clear the exposed particulate and repair the damaged tissue. The transcription factor NF-kB plays an important role in this host defense response as it regulates several downstream genes that modulate the immune and inflammatory processes.[58,59] Activation of this signaling pathway has been known to modulate the toxicity and pathological response to carbon black,[60] silica,[61] metal oxides,[62] high-aspect-ratio particulate-like asbestos,[56] single-walled nanotubes,[63] and multi-walled CNTs[64,65] exposure.

Quantitative assessment of NF-kB activation after exposure to hBN, AP-, BR-, W1-, and W2-BNNTs was performed using THP-1 NF-kB reporter cells at exposure concentrations of 0–100 μg mL^{-1} (**Figure 6**A). These cells secreted embryonic alkaline phosphatase (SEAP) when NF-κB signaling pathway becomes activated due to particulate exposure. After 12 h, challenge with the particulate, the levels of NF-kB induced was assessed by measuring SEAP in the cell culture supernatants and was compared with controls cells with no challenge. The lower purity BNNTs (AP and BR) and hBN did not induce significant change in the NF-kB at all the doses challenged. There was a dose-dependent increase in NF-kB induction with the high purity BNNT, W1 and W2. All the doses evaluated induced NF-kB significantly with W2 exposure while the highest two doses caused significant induction with W1 exposure. At the highest dose evaluated, W2 and W1 caused ≈ 33- and 18-fold increase in NF-kB induction compared to control cells with no exposure. Like cytotoxicity and membrane-damage responses, screening for NF-kB induction showed that only the highest-grade purity BNNT, which had the highest amount of high-aspect-ratio particulate, clustered with a significant response while hBN, AP-BNNTs, and boron-removed BNNTs (BR-BNNTs) clustered together, giving no response.

2.4.2. NLRP3 Inflammasome Activation

NLRP3 inflammasome activation plays an important role in the innate immune response to microbial and particulate exposure. Spherical particulate-like silica,[66] high-aspect-ratio material including BNNT,[26] CNTs,[67] asbestos,[68] and some lysosome-destabilizing nanomaterials,[69] are known to activate NLRP3 inflammasome complex that initiates pyroptosis and triggers the release of proinflammatory cytokines IL-1β and IL-18. The ability of hBN and various purity grade BNNTs to promote NLRP3 inflammasome activation was assessed by using the THP-1 inflammasome model where the monocytes are differentiated to macrophages and co-challenged with lipopolysaccharide (LPS) along with the particulate. Inflammasome activation was evaluated by measuring the released IL-1β and 1L-18 in response to 0–100 μg mL^{-1} challenge of the five particulates (Figure 6B,C). There was a general increase in secretion with increasing dose and all the BNNTs induced a significant increase in IL-18 production at 25 μg mL^{-1} and above concentrations. hBN induced a significant induction only at the highest dose, 100 μg mL^{-1}. Like IL-18, IL-1β induction was also significant at the highest dose for hBN and at 25–100 μg mL^{-1} for W1- and W2-BNNTs. BR-BNNT caused significant change from 6.25 μg mL^{-1}, while AP-BNNT did not induce significant alteration in IL-1β secretion at all the doses evaluated. At the highest dose evaluated, the magnitude of IL-18 increase was the greatest for the highest purity BNNTs (W1 and W2). The magnitude of AP- and BR-BNNTs response was similar and lower than the higher purity BNNTs. This increase can potentially be attributed to presence of higher amount of high-aspect-ratio particulate in the purer BNNTs.

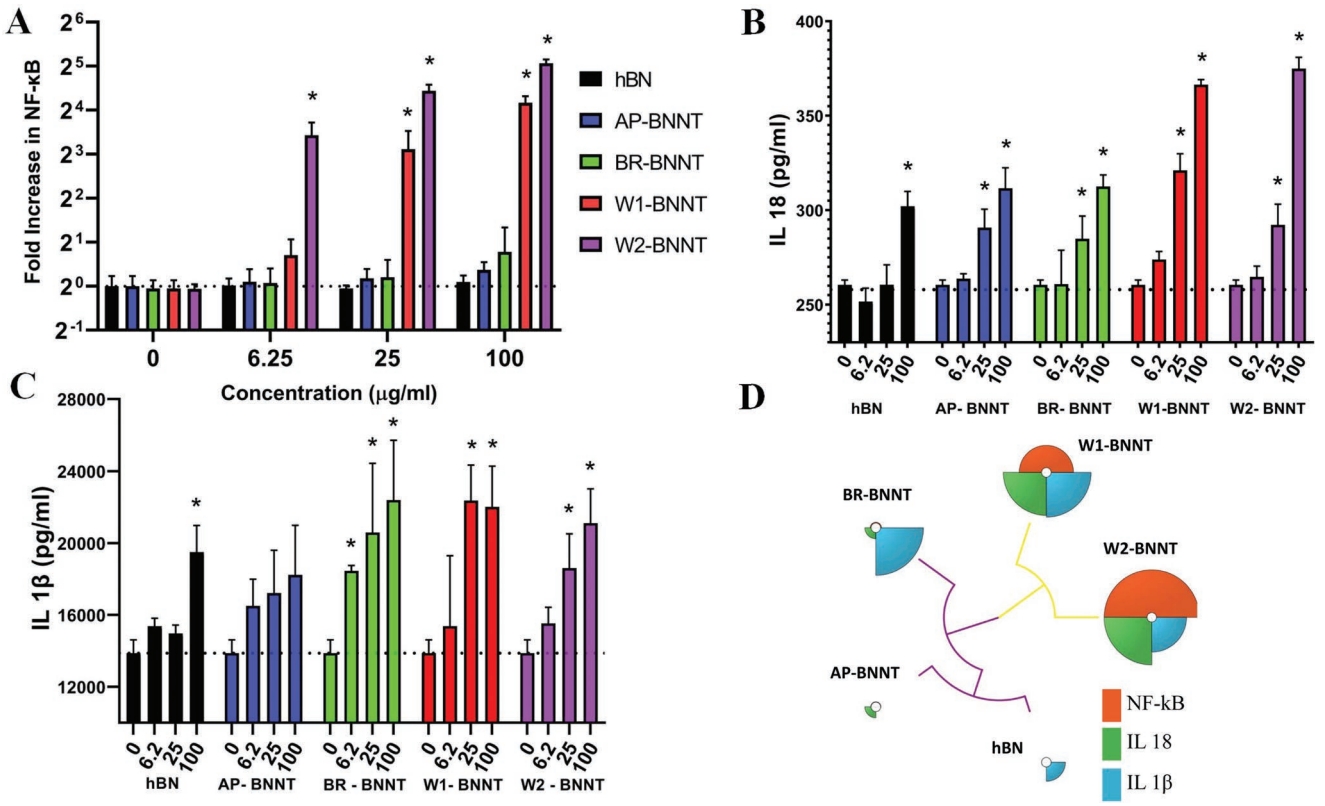

Figure 6. Mechanism-based screening of hBN and various purity grade BNNTs. A) NF-kB activation and inflammasome markers B) IL-18 and C) IL-1β secretion after exposure to 0–100 μg mL^{-1} of various test particulate. * highlights statistical significance ($p < 0.05$) from control cells with no exposure determined by two-way ANOVA analysis followed by pairwise comparison using Tukey's multiple comparisons test. D) Integrative visualization of the mechanism-based screening using toxicological priority index. Similarity in the response to mechanism-based screening was realized by unsupervised hierarchical clustering.

The integrated response of the NF-κB and NLRP3 inflammasome screening was analyzed and visualized using the ToxPi framework.[70] The response from NF-κB screening was given 50% weight and the inflammasome cytokine responses of IL-1β and IL-18 was each given a weight of 25%. Figure 6D shows the ToxPi profile of hBN, AP-, BR-, W1-, and W2-BNNTs clustered based on their similarity. The Integrative ToxPi priority scores were 0.08, 0.04, 0.3, 0.72, and 0.93 for hBN, AP-, BR-, W1-, and W2-BNNTs, respectively. The ToxPi clustergram visualized in Figure 5B clearly shows a marked difference in the response of W1 and W2 BNNTs and the others. With the second cluster there was a mark difference in boron removed BNNT from AP-BNNT and hBN precursor. The Ward-based Hierarchical clustering was also confirmed with K-Means clustering. The rank order based on the integrative ToxPi approach was W2-BNNT > W1-BNNT > BR-BNNT > hBN > AP-BNNT. The integrative score, rank order, scaled score for each of the responses, and the clustering groups have been included in Table S1, Supporting Information.

2.5. Alteration in Cytokine and Chemokine Secretions

Cytokine and chemokines are mediators of inflammation. The immune cells, predominantly macrophages, produce these as a response to infections, particulate exposure, or other insults. Macrophages use these secretions to help them regulate the microenvironment and recruit other cells. The immunomodulatory ability of various purity grade BNNT and hBN was screened by evaluating alteration in 46 proteins comprised of cytokines, chemokines, growth factors, and pro- and anti-inflammatory proteins. Macrophage differentiated THP-1 cells were challenged with 0, 6.25, 25, and 100 μg mL^{-1} of various purity grade BNNT for 24 h and the secreted proteins in the supernatant were evaluated (**Figure** 7A). The least number of statistically significant alterations in proteins was observed with hBN and this was observed at all the doses evaluated. The highest alterations were observed with W2 at the lowest two doses and with W1-BNNT at the highest dose. Considering the total number of altered proteins, the rank order across the treatment of groups and exposure concentrations was hBN < AP-BNNT < BR-BNNT < W1-BNNT < W2-BNNT. NF-κB is a potent transcription factor that is known to modulate macrophage phenotype and trigger a cascade of signaling events including cytokine and chemokine production.[71] The lack of a remarkable response in protein secretions is in line with the NF-κB screening performed earlier that showed only significant alteration in NF-κB with the highest purity BNNTs (W1 and W2).

The largest increase in expression across all the doses and particles was seen with fibroblast growth factor (FGF-2), which

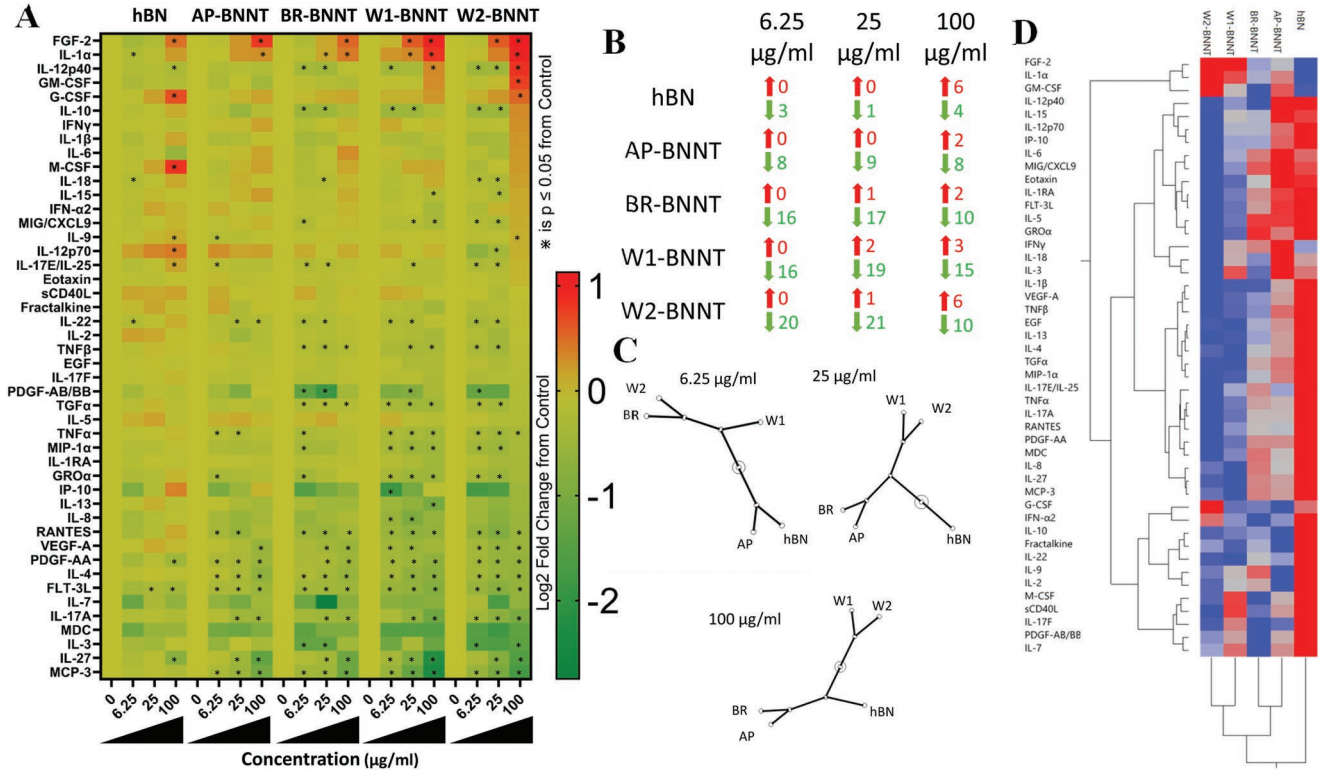

Figure 7. A) Heat map visualization of fold change in protein secretions in supernatant of differentiated THP-1 macrophages after challenge of 6.25, 25, and 100 μg mL^{-1} of hBN and various purity grade BNNTs compared to control cells with no exposure. * Highlights statistical significance ($p < 0.05$) by pairwise comparison to control cells identified by Student's *t*-test. B) Proteins significantly upregulated (Red) and downregulated (Green) after exposure to 6.25, 25, and 100 μg mL^{-1} of hBN and various purity grade BNNTs compared to control cells with no exposure. C) Constellation plot of the ward-based hierarchical cluster analysis of the protein expression at exposure of 6.25, 25, and 100 μg mL^{-1} of hBN and various purity grade BNNTs. D) Unsupervised hierarchical two-way clustering across exposure type and protein expression at 25 μg mL^{-1}.

was approximately two-fold following W1- and W2-BNNT exposure. With all the treatment groups, there was a dose-dependency in the number of proteins that were upregulated. At the highest dose, approximately six proteins were increased by hBN and W2-BNNT exposure. Compared to control cells with no exposure, the two high purity BNNTs caused a more than four-fold decrease in the magnitude of expression with some proteins. Compared to controls, there were more proteins that were significantly downregulated than upregulated with all treatments and concentrations (Figure 7B). The highest downregulated proteins were observed with W2-BNNT exposure at 25 μg mL^{-1} and the lowest were observed at the same exposure concentration with hBN. Unlike the upregulated proteins, there was no dose-dependency in the number of proteins that were downregulated with all the treatment groups.

Unlike what was observed with the THP-1 inflammasome model, there was no alteration in IL-1β secretion with all the purity grade BNNTs at all the doses evaluated. The in vitro model employed for screening inflammasome activation potential of the particulate utilized LPS co-stimulation (priming) to compensate for lack of pathogen-associated molecular patterns or danger-associated molecular patterns in the in vitro exposure conditions.[72,73] The absence of pro-IL-1β transcription due to absence of LPS cell priming is mostly likely the reason for the lack of significant response in IL-1β from non-primed differentiated macrophages.

A non-supervised two-way hierarchical cluster analysis (HCA, Ward method) was performed to segment the immunomodulatory response of various BNNTs to understand the effect of purity, group the treatment, and protein responses. For all the exposed particulate, clustering the response across the doses showed that the highest exposure dose, that is, 100 μg mL^{-1}, caused a distinct response and exposure to 6.25 and 25 μg mL^{-1} caused similar responses. At 25 μg mL^{-1}, there was less than 20% cytotoxicity with all the particulate treatment groups. Clustering the protein response at this exposure concentration (Figure 7D), we broadly observed the protein response to be segmented into two groups with respect to the treatments. The first group, consisting of three proteins FGF-2, IL-1α, and granulocyte macrophage colony stimulating factor (GM-CSF), revealed an upregulation in expression with increasing purity of the BNNT. With change in exposure dose, that is, at 6.25 μg mL^{-1} (Figure S6, Supporting Information) or 100 μg mL^{-1} (Figure S7, Supporting Information), other proteins including interferon gamma (IFNγ), IL-6, IL-7, and IL-18 joined this cluster that was characterized by a general upregulation with increasing BNNT purity. The second group consisted of the major portion of the proteins screened. Most of the proteins in the cluster showed a trend in decreasing protein secretions with increasing purity grade. In the cluster, hBN caused the highest level of secretion and the highest-grade purity BNNTs led to the lowest level of secretion. Several proteins including tumor necrosis factor

α (TNFα), IL-4, IL-17a, RANTES, platelet-derived growth factor AA (PDGF-AA), vascular endothelial growth factor A (VEGF-A), TNFβ, macrophage inflammatory protein 1 alpha (MIP-1α), IP-10, and monocyte chemotactic protein-3 (MCP-3) are part of this cluster. These proteins are involved in promotion of inflammation, tissue repair, and recruitment of other cells to assist in restoring homeostasis.

A constellation plot of the dendrogram obtained from HCA clustering at each dose (Figure 7C) showed that at the lowest dose, where there was the least number of altered mediators, and at the concentration where toxicity was not significantly induced, hBN and AP-BNNT formed a group and a second group consisted of BR-, W1-, and W2-BNNTs. Within the second group, the response of BR and W2 was more similar. At 25 μg mL^{-1}, the concentration at which cytotoxicity was significant, the response to hBN was markedly different from BNNTs and within the BNNTs, AP and BR caused a similar response and differed from the response of W1 and W2. Similar to 25 μg mL^{-1}, W1 and W2 had a similar response at 100 μg mL^{-1} but were markedly different from other materials. The second group consisted of hBN, AP, and BR. Within this group AP- and BR-BNNTs had a similar response. Taking into account the response of the highest two doses, where there was the maximum significant alterations and maximum magnitude in change in protein secretions, there were three groups. W1 and W2, the highest purity grade BNNTs, formed a group followed by a second group consisting of AP- and BR-BNNTs. The last distinct group was formed by hBN. There was a general trend that showed depression in protein expression with increasing purity. The release of cytokines was for the most part not robust and we have not observed any distinct macrophage polarization signatures with any of the particulate treatments. The alteration in the response was in line with the other endpoints like cytotoxicity and mechanism-based screening.

2.6. Functional Alteration in Macrophage Response

Epidemiology studies show that pulmonary exposure to air pollution particulate has been associated with a spike in hospitalization rates and secondary lung infections.[74–76] This functional alteration in macrophage innate immune response has been observed after exposure to various occupational particulates, such as nanomaterials including high-aspect-ratio materials like CNTs and BNNTs both in in vitro and animal models.[26,77–83]

Functional alteration due to exposure to hBN and various purity grades of BNNT was evaluated by exposing differentiated THP-1 macrophages to 0, 6.25, 25, and 100 μg mL^{-1} of various materials for 24 h, challenging them with recombinant *Escherichia coli* (*E. coli*) bacteria expressing green fluorescent protein (GFP) for 2 h, and quantifying the change in uptake by the macrophages. There was no suppression in bacterial uptake with all the test groups at all the concentrations evaluated (**Figure 8**). hBN simulated uptake with the highest two doses. There was a simulation in uptake after exposure of all BNNTs at the lower dose and at all doses with BR-BNNT (gas purified BNNTs). This stimulation in bacterial uptake after exposure to low cytotoxic concentrations may be due to shared receptors involved in uptake of bacteria and nanomaterial. Nanoparticles and

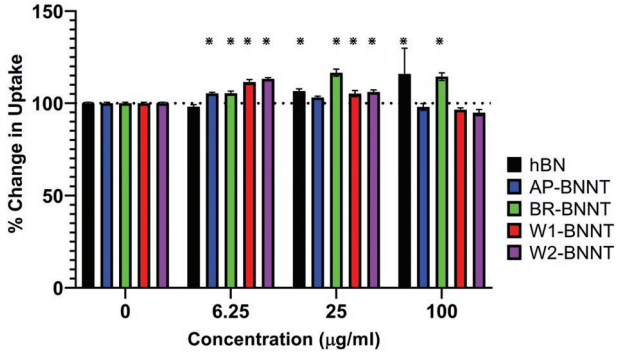

Figure 8. Change in GFP *E. coli* uptake after pre-challenge with 6.25, 25, and 100 μg mL^{-1} of hBN and various purity grade BNNTs. * Highlights statistical significance ($p < 0.05$) by pairwise comparison to control cells with no exposure.

bacteria share common uptake receptors like scavenger receptors and MARCO;[84] the macrophages exposed to non-cytotoxic nanomaterial may stimulate the amount of receptors present on the surface in a bid to achieve homeostasis and this increase in receptors may be responsible for enhancing the bacterial uptake. An increase in scavenger receptors has been seen after exposure to non-cytotoxic concentration of some nanomaterial like ZnO.[85] Further work involving characterizing the surface receptors after exposure to BN group of material is needed to confirm if alteration in surface receptors is responsible for the simulation in bacterial uptake observed.

The lack of suppression in phagocytic capacity after pretreatment with BNNTs suggests that BNNTs produced via HABS are relatively nontoxic in terms of altering the macrophage response and that the various steps of purification did not further depress the response.

3. Conclusion

The BNNTs were manufactured by HABS method and involves an atmospheric-pressure, high-temperature plasma process utilizing an hBN powder feedstock. The AP-BNNT was fibrous, sheet- and powder-like, brown in color (Figure S2, Supporting Information) and contained 50% BNNT by weight and the balance composed of low aspect ratio particulate, elemental boron (≈25 wt%) and hBN derivatives (≈25 wt%). AP-BNNT was reacted with chlorine gas (at 750 °C) to remove free boron and was named BR. Apart from color change (Figure S2, Supporting Information), spectroscopy characterization confirmed removal of elemental boron in BR-BNNT. This material was further purified by washing with water and acetone in sequential steps, sonication and filtering them through a 20 μm stainless steel filter. The washed samples were referred to as W1 and W2; W2 had progressively more wash steps. XPS confirmed increasing BN content and decreasing BO content after each sequential step of the purification. SEM confirmed fewer low-aspect-ratio features as the material moved from AP-BNNT to BR-BNNT to W-BNNT. EPR showed that there is a decrease in surface oxidant radical production with increasing purity. This was pronounced with hBN and AP-BNNT. The reactivity inversely correlated to total surface area, purity of the

BN material (XPS %BN area) and directly correlated to surface oxygen (XPS %BO), suggesting that BNNT was not responsible for the oxidant production leaving oxidant impurities/residuals in the sample responsible for the radical production.

The BNNT materials were not overtly toxic. Cytotoxicity and membrane damage occurred only at the higher concentrations and was dependent on the purity grade of the BNNTs. Solvent-washed and filtered BNNT (W1 and W2) grouped together and caused the most significant cytotoxicity among all the tested materials. hBN, AP-, and BR-BNNTs clustered together and within this cluster, BR-BNNT clustered separately. As evident from the BMD, the gas purified BR-BNNT (boron removed) had the lowest toxicity. There are primarily two potential hazards that can influence the toxicity response of these material, the first one from oxidant radicals generated by impurities/residuals and the second from shape of the material, that is, aspect ratio of material. Based on the toxicity response, shape/aspect ratio seemed to be a major influence on the toxicity response of BNNTs. This is in line with previous toxicity studies with BNNT manufactured with the HABS method that showed that the increase in length of BNNTs correlated with toxicity in cardiomyocytes.[28] HABS manufacturing process is unique as it employs a relatively high-partial pressure of hydrogen (15–30 vol%) to produce various B—N—H intermediate species that catalyze the growth of BNNT. These B—N—H byproducts are present in AP-BNNTs. With AP-BNNT having lower toxicity compared to purer forms of BNNT, it can be assumed that the B—N—H byproducts are not causing additional toxicity. In general, oxidant impurities/residuals predominantly present in hBN and AP-BNNT do not appear to have a significant influence on the toxicity. The toxicity was assessed on equal mass basis and hBN had almost tenfold higher density and a corresponding decrease in total surface area; as such, masking of the oxidant induced toxicity response in hBN and AP-BNNT due to density should not be negated. Screening for the mechanism of toxicity induced by various BN materials was performed by evaluating the dose-response relationship of NF-κB and their potential for inflammasome activation. There was a dose-response relationship in NF-κB activation with only the highest purity BNNTs (W1 and W2). The potential for inflammasome activation was observed with all the purity grade BNNTs (BR, W1, and W2), while activation was observed only at the higher doses with hBN and AP-BNNT. This response can be due to increased presence of high-aspect-ratio material with increasing purity of BNNT material. The integrative mechanism-based scoring and clustering through ToxPi showed similar grouping as observed with cytotoxicity where the highest purity (W1 and W2) clustered together and the response from hBN, AP, and BR clustered, with BR having a slightly different response compared to hBN and AP.

Macrophage inflammatory response after exposure to BN material was evaluated by multiplex measurement of 48 proteins in supernatants after exposure to 0–100 μg mL^{-1} for 24 h. The protein secretions were not remarkable and a significant, general downregulation in protein alterations was observed with all the tested materials. Hierarchical clustering of the protein response at 25 and 100 μg mL^{-1} confirmed the clustering observed with cytotoxicity and mechanism-based screening where the response of W1 and W2 clustered together followed by a second cluster that consists of hBN, AP, and BR. Within this cluster BR clustered with AP at the higher two dose and at the lowest dose clustered with W1 and W2 cluster. Exposure to BN materials did not cause any suppression in macrophage phagocytic capacity at all the doses evaluated. There was a stimulation in bacteria uptake with the highest two doses of hBN, the lower dose with all BNNTs, and with BR at all the doses evaluated. The reason for the stimulation in uptake needs to be investigated further.

Taken together, the data suggests that hBN or BNNT materials manufactured through HABS in general are not overtly immuno-toxic as evident from the unremarkable inflammatory protein secretion responses and the lack of suppression of macrophage function. There was a clear clustering in cytotoxicity, mechanism-based screening, and inflammatory response with purity of the material. With increasing purity of BNNT there was a gradient in toxicity, and this may be attributed to the presence of more higher aspect ratio material with increasing purity grade. The differential toxicity observed with various purity grades further affirms that the conflicting reports and difference in toxicity reported in the literature may be partially attributed to various purity grades of BNNT utilized in the studies.

4. Experimental Section

Synthesis of Boron Nitride Nanotubes and Purification: BNNTs were synthesized by the HABS method as described by Kim et al.[22,23] Briefly, the method was an atmospheric pressure, high-temperature plasma process utilizing an hBN powder feedstock (70 nm; MK-hBN-N70, MK Impex Corp.) and a relatively high partial-pressure of hydrogen (15–30 vol% H_2 in Ar/N_2/H_2), which catalyzes the growth of BNNTs through formation of B—N—H intermediate species. The synthesis product, a combination of fibrous, sheet- and powder-like material, was brown in color due to the presence of elemental boron as an impurity (Figure S2, Supporting Information). This material was homogenized by mechanical grinding to produce the BNNT material referred to as-produced or AP-BNNTs in the present study. This fluff-like material was commercialized as BNNT-R by Tekna Advanced Materials (Sherbrooke, Quebec, Canada) and was estimated to contain 50% BNNTs by weight. The balance was composed of elemental boron (≈25 wt%) and hBN derivatives (≈25 wt%) present as low-aspect-ratio particles.

In addition to AP-BNNTs, purified BNNT samples (see Table 2) were produced and assessed. AP-BNNTs were first purified by a gas-phase process to chemically remove the boron impurity. The resulting material, referred to here as BR-BNNTs, was obtained through reaction of the boron impurity with chlorine gas at high temperature (750 °C) as recently reported.[16] Briefly, the boron impurity was converted to BCl_3 gas, according to

$$2B_{(s)} + 3Cl_{2(g)} \rightarrow 2BCl_{3(g)} \quad (1)$$

and was removed in the flow (Cl_2, N_2, and Ar gas) and neutralized with an aqueous solution. The BR-BNNTs were further purified using increasing amounts of solvent washing (see Table 2) yielding samples referred to as "washed" or W-BNNTs. Washing began with 22.5 g BR-BNNTs, which were divided between three 4 L bottles (7.5 g each). In each wash cycle, the BNNT material was dispersed in 4 L clear solvent (water or acetone) using bath sonication (15 min). The combination of water followed by acetone appeared to be advantageous, as water preferentially solubilized/dispersed some impurities in the BNNT samples but extended sonication in water was observed to damage BNNTs. The sonication was necessary to separate impurities from

the nanotubes, which results in a milky white suspension. The liquid was removed by filtration (20 µm stainless steel mesh) to recover the nanotube material. The filtrate was kept wet by spraying with clean solvent to prevent drying and minimize aggregation during the filtration step, after which it was re-dispersed in clean solvent to repeat the cycle. As the number of wash cycles increased, the liquid after sonication appeared less milky indicating a reduction in impurities relative to the original BR-BNNTs. However, yields also dropped from ≈40–50% for 6 cycles to <10% for 16 cycles. In addition to the series of progressively more purified BNNTs (AP to BR to W), a second washed sample, called "washed 2" or W2-BNNTs was also produced; this sample was derived from a different batch of BR-BNNTs and was subjected to additional wash cycles (eight acetone washes instead of four washes with W1-BNNTs). Toxicological evaluation of this sample allowed determining alterations in toxicity profile between batches with minor alterations. After conclusion of the washing cycles for each sample, the material was dispersed in water, frozen, and freeze-dried, which reduced aggregation in comparison to air-dried samples and was helpful for re-dispersion, to recover a fluff-like BNNT powder. hBN nanoparticles (≈100 nm) from SkySpring Nanomaterials Inc. (Houston, TX, # 1522DX) were used as a low aspect ratio material control for the toxicity screening.

Thermogravimetric and Spectroscopic Characterization: The set of BNNT materials was characterized by coupled thermogravimetric analysis with Fourier transform infrared spectroscopy (TGA-FTIR), infrared spectroscopy, SEM including with energy dispersive X-ray spectroscopy (SEM–EDX), and XPS. TGA in air, and coupled TGA-FTIR under argon, were performed at a heating rate of 10 °C min^{-1} with a Netzsch STG 449 F1 TGA instrument coupled to a Bruker Tensor 27 FTIR spectrometer. In addition to FTIR spectra of the species desorbed during TGA, infrared spectra of the BNNT materials were measured in reflectance mode using attenuated total reflectance FTIR (ATR-FTIR, Agilent 630 FTIR) on paper-like BNNT material samples, produced by dispersion of methanol with minimal sonication (10 min) and filtration. The same paper-like samples were used for XPS (Kratos AXIS Ultra DLD spectrometer, 1486.6 eV monochromated Al K-alpha beam, 5×10^{-9} Torr) and SEM-EDX (Hitachi S4700). XPS measurements used a spot size of 700 µm × 300 µm, the largest possible for the instrument, and two spots were measured for each sample, to ensure the spectra were representative of the average for the sample.

Surface Area and Density: Surface area of the particulates was measured on the powder form by gas adsorption using a Micromeritics ASAP2020 (Micromeritics Instrument Corporation, Norcross, GA) surface area analyzer. Samples were degassed in ultrahigh purity (UHP) nitrogen for 30 min at 90 °C, and then for 90 min at 200 °C. The surface areas were determined by multipoint point BET method[86] with UHP nitrogen as the adsorbate and liquid nitrogen as the cryogen.

For measuring the tapped density, a 10 mL graduate cylinder was tared on a calibrated analytical balance and the material was added. To measure tapped density, the container was tapped 3000 times, for three runs, using a Quantachrome Autotap (Anton Paar QunataTec Inc., Boynton Beach, Florida). The level of the particulate was recorded to the nearest 0.1 mL. The cylinder with particulate was reweighed. Density was calculated as the mass of particulate divided by volume of the particulate.

Length and Diameter: Length and diameter of the tubes was measured using high resolution scanning transmission electron microscopy. Transmission electron microscopy grid was dipped into the particulate dispersion prepared by sonicating the BNNT in isopropanol for 5 min. Imaging was performed on a Hitachi HD-2300 STEM. Length was determined by connected points at the two extremes without following the curvature of the nanotube or nanofiber. 200 measurements were made to determine the length and diameter.

Two-Dimensional Agglomerate Sizing: The agglomerated dimension of BNNT in dispersion media (DM) was determined using field emission SEM (Hitachi S-4800, Tokyo, Japan). The largest crosswise diameter of 75 agglomerates was measured for each material. Materials were subsequently categorized into distinct groups of agglomeration defined as either spherical agglomerates or bundles of fibers with one dimension greater than three times the other dimension, referred to as bundled agglomerates. Bundled agglomerates had both a diameter and length measurement.

Cell Culture: Human peripheral blood monocyte cell line, THP-1 cells, were cultured, differentiated, and primed using procedures described previously by Xia et al.[72] In brief, human monocyte THP-1 cells (ATCC # TIB 202) were grown in growth media containing RPMI-1640 media supplemented with 10% fetal bovine serum, 100 µg mL^{-1} Penicillin-Streptomycin, and 50 µM of beta-mercaptoethanol. Cells were cultured in an incubator maintained at 37 °C and 5% CO_2. THP-1 cells were differentiated into macrophages by treating them with growth media containing vitamin D3 at 150 nM for 48 h and then 5 nM phorbol 12-myristate 13-acetate (PMA) for 12 h. For inflammasome activation, the differentiated THP-1 cells were primed to induce the transcription of pro-IL-1β by co-treating them with 10 ng mL^{-1} LPS when challenging with the nanomaterial. NF-κB SEAP Reporter Monocytes (THP 1-Blue NF-κB Cells, Invivogen Inc., San Diego, CA) were cultured and differentiated like THP-1 WT cells described above. 10 µg mL^{-1} of blasticidin (Invivogen) was added to the growth media to maintain selection. All experiments were conducted on cells with passage 20 or below. Cell cultures were tested and found to be negative for mycoplasma contamination.

Dispersion in Cell Culture Media, Hydrodynamic Size, and Zeta Potential: BNNTs were highly hydrophobic. To prepare aqueous dispersion of these materials for toxicity studies, the four BNNTs and the hBN material were weighed and suspended in 100% ethanol at 1 mg mL^{-1} in glass vials. The glass vials were sonicated for 5 min in a cup-holder sonicator. Samples were dried to remove ethanol in an oven maintained at 120 °C for 4 h. Stock aqueous dispersions were prepared in DM containing mouse serum albumin (0.6 mg mL^{-1} final concentration) and 1,2-dipalmitoyl-*sn*-glycero-3-phosphocholine (DPPC; 10 µg mL^{-1}) at 5 mg mL^{-1} particle concentration in United States Pharmacopeia-grade phosphate buffered saline. DM was a simplistic replication of the lung lining fluid and were shown to be a good dispersant for evaluating in vivo pulmonary toxicity after exposure to various high aspect ratio occupational nanomaterial exposures.[87–89] The dispersion for in vitro use was also prepared in DM to allow future comparison of the in vitro bioactivity with the in vivo pathological outcomes. The stock dispersions were prepared by sonicating for 3 min at 70% amplitude using a cup-horn sonicator (Sonics VibraCell VCX-750 with cup-type sonicator; Newton, CT) immersed in continuous flowing cold water. The samples were vortexed intermittently after every min for 10 s. The DM dispersed stock particulate were further diluted to 100 µg mL^{-1} in cell culture medium (highest test concentration), sonicated, and probe-tip sonicated (Branson Sonifer 450, continuous output) for a total of 1 min, with 10 s vortexing after every 30 s. Other concentrations were achieved by serial dilution.

DLS was used to measure agglomerate hydrodynamic size and charge of the agglomerates (zeta potential). A Malvern Zetasizer Nano ZS90 (Worcestershire, UK) equipped with a 633 nm laser at a 90° scattering angle was used for the DLS measurements. Stock dispersions were prepared in DM at 5 mg mL^{-1} and all measurements were performed at a particle concentration of 25 µg mL^{-1} in cell culture growth medium, while maintaining a constant temperature of 25 °C. Samples were equilibrated inside the instrument for 2 min, and five measurements, each consisting of at least five runs, were recorded.

Electron Microscopy Verification of Particle Internalization: THP-1 monocytes were differentiated to macrophages and challenged with 25 µg mL^{-1} of hBN, AP-, and W2-BNNT for 24 h. After the exposure period, cells were washed thrice with PBS and fixed with Karnovsky's fixative buffered in 0.1 M sodium cacodylate. The cells were later post-fixed in 1% osmium tetroxide; stained en bloc with 1% tannic acid and 0.5% filtered uranyl acetate; dehydrated with a graded series of ethanols; infiltrated with propylene oxide and LX-112 epon; and embedded in LX-112 epon. Sections were cut at 70 nm, placed on 200 mesh copper grids and stained with 4% uranyl acetate and Reynolds' lead citrate. Images were taken using a JEOL JEM 1400 transmission electron microscope (JEOL USA) with an AMT XR-81 M-B digital camera attachment.

Cytotoxicity and Membrane Damage: THP-1 monocytes were differentiated with Vit D3/PMA as described in the cell culture section and the differentiated macrophages were challenged with 100 µL of fresh growth media containing 0, 1.56, 3.125, 6.25, 12.5, 25, 50, and 100 µg mL^{-1} of hBN, AP-BNNT, BR-BNNT, W1-BNNT, and W2-BNNT for 24 h. Membrane damage was assessed by evaluating the LDH released using CytoTox-ONE Homogeneous Membrane Integrity Assay (Promega Inc, Madison, WI). In parallel, cytotoxicity due to the particulate exposure was assessed using cell's ability to reduce tetrazolium salt WST-1 (Sigma-Aldrich, St. Louis, MO). Fresh media containing 10% WST-1 was given after 24 h of nanoparticle exposure and after 2 h of incubation, the WST-1 consumption was recorded by measuring the absorbance at 450 nm subtracted with absorbance at 660 nm to account for turbidity/background. Data were presented as percent change from control cells with no particulate treatment. Total LDH in the cells was evaluated by lysing the cells with 0.1% Triton X-100 (Sigma-Aldrich) for 1 h. Equal volumes of cell culture medium and CytoTox-ONE Reagent (Promega, Madison, WI) were reacted at room temperature and the change in fluorescence was measured at excitation 560 nm and emission 590 nm. All experiments were repeated three times, and each measurement had quadruplicate technical replicates. BMD, benchmark lower confidence limit (BMDL), and benchmark upper confidence limit (BMDU) were estimated using the cytotoxic WST-1 dose-response relationship data using Benchmark Dose Response Software (BMDS).[90]

Endotoxin: Endotoxin contamination on the particulate was evaluated using Pierce Chromogenic Endotoxin Quant Kit (Thermo Fisher Scientific, MA; # A39552) as per manufacturer's recommendation. The procedure was based on amebocyte lysate method that measured the endotoxin levels by measuring its interaction with proenzyme Factor C. The range of sensitivity for endotoxin detection was 0.12–1.0 EU mL^{-1}.

Caspase 3/7: Apoptosis due to particulate exposure was quantified by evaluating active caspase 3 and 7 using FLICA 660 Caspase 3/7 (ImmunoChemistry Technologies Inc, #9125). Once activated, caspases 3 and/or 7 cleaved protein substrates leading to apoptosis and cell death. The fluorescent caspase 3/7 probe used contained Asp–Glu–Val–Asp (DEVD) that binds active form of the caspase enzymes. Differentiated THP-1 macrophages were challenged for 48 h with 0, 12.5, and 100 µg mL^{-1} of hBN and the purified BNNT, W2-BNNT. The fluorescent intensity was quantified by measuring fluorescent intensity using Varioskan LUX multimode microplate reader (Thermo Fisher Scientific Inc, MA). The fluorescent intensity was normalized by labeling cell nuclei with cell-permeant nuclear counterstain Hoechst 33342 (ImmunoChemistry Technologies Inc, #639).

Electron Paramagnetic Resonance: Acellular reactivity and test materials ability to generate free radical intermediates was evaluated by EPR spin-trapping. The particulates were exposed to H_2O_2 and their ability to produce hydroxyl radicals (OH·) through a Fenton-like reaction was evaluated. 5,5′-Dimethylpyrroline N-oxide (DMPO, 100 mM, Sigma-Aldrich), various BNNTs (5 mg mL^{-1}), hBN (5 mg mL^{-1}) or potassium dichromate (2 mM), and H_2O_2 (1 mM) were suspended in PBS and mixed in the order listed. All reagents were mixed in test tubes for 3 min at room temperature, filtered through a Titan3 nylon 0.45 µm filter to halt the reaction, and filter any particulate. EPR measurements were performed on a Bruker EMX spectrometer (Bruker Instruments Inc., Billerica, MA) using a quartz flat cell. Samples were run in independent experiments, $n = 3$. Three technical replicate scans were performed for each run and each scan was performed for 41 s with a receiver gain of 10^4, a 40 ms time constant, 1.0 G modulation amplitude, 63.4 mW power, 9.751 frequency, and 3515 G magnetic field center. Sample data was attained and processed as previously described.[91,92] Briefly, signal intensity (peak height) from the 1:2:2:1 spectra, which was characteristic of the OH· radical,[93] was used to measure the relative amount of short-lived radicals trapped.

Nuclear Factor-κB Activation: NF-κB activation due to particulate exposure was evaluated using THP1-Blue NF-κB cells (InvivoGen Inc., San Diego, CA). These cells were derived from human THP-1 monocyte cell line by stable integration of an NF-κB-inducible SEAP reporter construct. NF-κB activation was determined by measuring the induced SEAP levels in the cell culture supernatants. The differentiated macrophages were exposed to 100 µl of 0, 6.25, 25, and 100 µg mL^{-1} of hBN, AP-BNNT, BR-BNNT, W1-BNNT, and W2-BNNT for 12 h. The supernatants were centrifuged and SEAP in the supernatants was quantified by reacting the supernatant with QUANTI-Blue Solution (InvivoGen Inc.) and measuring the absorbance at 660 nm.

Inflammasome Activation: An inflammasome model was used to assess hBN and BNNTs potential for inflammasome induction. In this in vitro model, the macrophages were co-challenged with LPS along with the nanoparticles. Differentiated THP-1 macrophages were challenged with fresh media containing 10 ng mL^{-1} of LPS and 0, 6.25, 25, and 100 µg mL^{-1} of the various BNNTs or hBN for 24 h. The nanoparticles were co-treated with LPS to prime the macrophage monocultures to induce the transcription of pro-IL-1β and promote inflammasome activation. IL-1β and IL-18, markers for inflammasome activation were assessed using human IL-1β ELISA kit (R&D Systems, Minneapolis, MN, #DLB50) and IL-18 ELISA kit (MBL International, MA, # 7620) following the manufacturer's recommendations.

Inflammatory Protein Secretions: Differentiated THP-1 macrophages were challenged with growth media containing 0, 6.25, 25, and 100 µg mL^{-1} of the various BNNTs or hBN for 24 h. 48-protein multiplex cytokine analysis was performed on the supernatants by Eve Technologies (Eve Technologies, Calgary, Alberta, Canada). The 48-plex consisted of soluble CD40 ligand (sCD40L), epidermal growth factor, eotaxin, FGF-2, Fms-like tyrosine kinase receptor 3 ligand (Flt-3 ligand), fractalkine, granulocyte colony stimulating factor (G-CSF), GM-CSF, growth regulated oncogene α, human interferon alpha-2, IFNγ, interleukins (IL) IL-1α, IL-1β, IL-1ra, IL-2, IL-3, IL-4, IL-5, IL-6, IL-7, IL-8, IL-9, IL-10, IL-12p40, IL-12p70, IL-13, IL-15, IL-17A, IL-17E/IL-25, IL-17F, IL-18, IL-22, IL-27, interferon gamma-induced protein 10 (IP-10), monocyte chemoattractant protein-1 (MCP-1/CCL2), MCP-3, macrophage colony-stimulating factor, macrophage derived chemokine (CCL22), monokine induced by gamma, MIP-1α (CCL3), macrophage inflammatory protein-1β, PDGF-AA, PDGF-AB/BB, regulated upon activation, normal T cell expressed and presumably secreted (RANTES), transforming growth factor alpha, TNFα, TNFβ, and VEGF-A. The assay sensitivities for these markers ranged from 0.1 to 33.3 pg mL^{-1}.

Macrophage Phagocytosis Assay: Differentiated THP-1 cells were exposed to 0, 6.25, 25, and 100 µg mL^{-1} of hBN and various purity grade BNNTs for 24 h and were further challenged with fresh medium containing *E. coli* GFP (ATCC # 25922GFP) at multiplicity of infection of 1:25. In order for the bacteria to reach the cells at the bottom of the well, the plate containing the cells and bacteria was centrifuged at 300 × *g* for 10 min. After 2 h of challenge, the cells were washed with PBS, harvested by trypsinization and scraping, centrifuged at 1000 × *g* for 5 min and resuspended in PBS. The cell-associated bacteria were quantified using a BD LSR II flow cytometer (BD Biosciences, San Diego, CA). All experiments were performed using triplicate samples and at least 10 000 cells were analyzed per treatment.

Statistical Comparisons and Analysis: Statistical analyses were performed using either JMP version 13, or Prism 9 for Windows. Assays were analyzed using one-way (particle type) and two-way (particle type by dose) by factorial analyses of variance (ANOVA), followed by Tukey's multiple comparison test for pairwise comparisons based on the experimental design. For some variables, a natural log transformation was performed on the data to reduce heterogeneous variance and meet the assumptions of an ANOVA. United States Environmental Protection Agency's BMDS Version 3[90] was used to evaluate the BMD response. The Akaike Information Criterion (AIC) was used for model selection, and the model with the lowest AIC value was used to select the best model between the various models. A 10% change in the response rate of an adverse effect (cytotoxicity) relative to the response of control group was used as the benchmark response. The protein response was presented as heatmap of $\log_2$-fold change of the protein concentration and comparisons with controls was performed by Student's *t*-test. Hierarchical cluster analysis was performed by Wards method (Wards minimum variance clustering method).[94] A weight-based integrative scoring for the mechanism-based screening was performed using ToxPi graphical user interface.[70]

Supporting Information

Supporting Information is available from the Wiley Online Library or from the author.

Acknowledgements

The authors thank D. Ruth, M. Plunkett, and S. Walker from NRC's nanotube manufacturing facility, and M. Daroszewska (NRC), O. Naboka (NRC), and O. Kodra (NRC) for characterization support. Funding: this work was funded by National Institute for Occupational Safety and Health, Nanotechnology Research Center # 921043T. The production and characterization of BNNT materials was supported by the Security Materials Technology program of the National Research Council Canada. The findings and conclusions in this report are those of the authors and do not necessarily represent the official position of the National Institute for Occupational Safety and Health, Centers for Disease Control and Prevention. Mention of brand name does not constitute product endorsement.

Conflict of Interest

The authors declare no conflict of interest.

Data Availability Statement

The data that support the findings of this study are available from the corresponding author upon reasonable request.

Keywords

aspect ratio, boron nitride nanotubes, mechanism-based screening, NALP3 inflammasome, nuclear factor-κB, purity, residuals, toxicity

Received: May 25, 2022
Revised: August 25, 2022
Published online: November 14, 2022

[1] M. B. Jakubinek, B. Ashrafi, Y. Martinez-Rubi, J. Guan, M. Rahmat, K. S. Kim, S. Dénommée, C. T. Kingston, B. Simard, in *Nanotube Superfiber Materials*, 2nd ed., (Eds: M. J. Schulz, V. Shanov, Z. Yin, M. Cahay), William Andrew Publishing, Norwich, NY **2019**, pp. 91–111.
[2] D. Zhang, S. Zhang, N. Yapici, R. Oakley, S. Sharma, V. Parashar, Y. K. Yap, *ACS Omega* **2021**, *6*, 20722.
[3] J. H. Kim, T. V. Pham, J. H. Hwang, C. S. Kim, M. J. Kim, *Nano Converg* **2018**, *5*, 17.
[4] O. R. Lourie, C. R. Jones, B. M. Bartlett, P. C. Gibbons, R. S. Ruoff, W. E. Buhro, *Chem. Mater.* **2000**, *12*, 1808.
[5] J. Wang, V. K. Kayastha, Y. K. Yap, Z. Fan, J. G. Lu, Z. Pan, I. N. Ivanov, A. A. Puretzky, D. B. Geohegan, *Nano Lett.* **2005**, *5*, 2528.
[6] A. Pakdel, C. Zhi, Y. Bando, T. Nakayama, D. Golberg, *Nanotechnology* **2012**, *23*, 215601.
[7] K. S. Kim, G. Sigouin, H. Cho, M. Couillard, M. Gallerneault, S. Y. Moon, H. S. Lee, M. J. Kim, S. G. Jang, H. Shin, *ACS Omega* **2021**, *6*, 27418.
[8] A. Tiano, C. Park, J. Lee, H. Luong, L. Gibbons, S.-H. Chu, S. Applin, P. Gnoffo, S. Lowther, H. J. Kim, P. Danehy, J. Inman, S. Jones, J. H. Kang, G. Sauti, S. Thibeault, V. Yamakov, K. Wise, J. Su, C. Fay, *Boron Nitride Nanotube: Synthesis and Applications*, Vol. *9060*, SPIE, Bellingham, WA **2014**.
[9] C. S. T. Castillo, C. Bruel, J. R. Tavares, *Nanoscale Adv* **2020**, *2*, 2497.
[10] H. Harrison, J. T. Lamb, K. S. Nowlin, A. J. Guenthner, K. B. Ghiassi, A. D. Kelkar, J. R. Alston, *Nanoscale Adv* **2019**, *1*, 1693.
[11] S. Hales, J. Alexa, B. Jensen, Radio Frequency Plasma Synthesis of Boron Nitride Nanotubes (BNNTs) for Structural Applications: Part II. Center, N. L. R., Ed. NASA: Hampton, **2016**.
[12] G. P. Soares, S. Guerini, *J. Mod. Phys.* **2011**, *2011*, 857.
[13] M. S. Amin, T. E. Molin, C. Tampubolon, D. E. Kranbuehl, H. C. Schniepp, *Chem. Mater.* **2020**, *32*, 9090.
[14] L. Li, L. H. Li, Y. Chen, X. J. Dai, T. Xing, M. Petravic, X. Liu, *Nanoscale Res. Lett.* **2012**, *7*, 417.
[15] J. S. M. Nithya, A. Pandurangan, *RSC Adv.* **2014**, *4*, 26697.
[16] H. Cho, S. Walker, M. Plunkett, D. Ruth, R. Iannitto, Y. M. Rubi, K. S. Kim, C. M. Homenick, A. Brinkmann, M. Couillard, S. Dénommée, J. Guan, M. B. Jakubinek, Z. J. Jakubek, C. T. Kingston, B. Simard, *Chem. Mater.* **2020**, *32*, 3911.
[17] H. Chen, Y. Chen, J. Yu, J. S. Williams, *Chem. Phys. Lett.* **2006**, *425*, 315.
[18] M. S. Amin, B. Atwater, R. D. Pike, K. E. Williamson, D. E. Kranbuehl, H. C. Schniepp, *Chem. Mater.* **2019**, *31*, 8351.
[19] D. M. Marincel, M. Adnan, J. Ma, E. A. Bengio, M. A. Trafford, O. Kleinerman, D. V. Kosynkin, S.-H. Chu, C. Park, S. J. A. Hocker, C. C. Fay, S. Arepalli, A. A. Martí, Y. Talmon, M. Pasquali, *Chem. Mater.* **2019**, *31*, 1520.
[20] A. D. S. McWilliams, A. Carlos, L. Liberman, S. Ergülen, Y. Talmon, M. Pasquali, A. A. Martí, *Nanoscale Adv* **2019**, *1*, 1096.
[21] J. Ko, H. M. Kim, S. Y. Moon, S. Ahn, S. G. Im, Y. Joo, *Chem. Mater.* **2021**, *33*, 4723.
[22] K. S. Kim, M. Couillard, H. Shin, M. Plunkett, D. Ruth, C. T. Kingston, B. Simard, *ACS Nano* **2018**, *12*, 884.
[23] K. S. Kim, C. T. Kingston, A. Hrdina, M. B. Jakubinek, J. Guan, M. Plunkett, B. Simard, *ACS Nano* **2014**, *8*, 6211.
[24] Y. Huang, J. Lin, C. Tang, Y. Bando, C. Zhi, T. Zhai, B. Dierre, T. Sekiguchi, D. Golberg, *Nanotechnology* **2011**, *22*, 145602.
[25] M. W. Smith, K. C. Jordan, C. Park, J.-W. Kim, P. T. Lillehei, R. Crooks, J. S. Harrison, *Nanotechnology* **2009**, *20*, 505604.
[26] V. K. Kodali, J. R. Roberts, M. Shoeb, M. G. Wolfarth, L. Bishop, T. Eye, M. Barger, K. A. Roach, S. Friend, D. Schwegler-Berry, B. T. Chen, A. Stefaniak, K. C. Jordan, R. R. Whitney, D. W. Porter, A. D. Erdely, *Nanotoxicology* **2017**, *11*, 1040.
[27] X. Xin, M. Barger, K. A. Roach, L. Bowers, A. B. Stefaniak, V. Kodali, E. Glassford, K. L. Dunn, K. H. Dunn, M. Wolfarth, S. Friend, S. S. Leonard, M. Kashon, D. W. Porter, A. Erdely, J. R. Roberts, *NanoImpact* **2020**, *19*, 100235.
[28] J. Augustine, T. Cheung, V. Gies, J. Boughton, M. Chen, Z. J. Jakubek, S. Walker, Y. Martinez-Rubi, B. Simard, S. Zou, *Nanoscale Adv* **2019**, *1*, 1914.
[29] L. Horváth, A. Magrez, D. Golberg, C. Zhi, Y. Bando, R. Smajda, E. Horváth, L. Forró, B. Schwaller, *ACS Nano* **2011**, *5*, 3800.
[30] G. Ciofani, S. Del Turco, A. Rocca, G. de Vito, V. Cappello, M. Yamaguchi, X. Li, B. Mazzolai, G. Basta, M. Gemmi, V. Piazza, D. Golberg, V. Mattoli, *Nanomedicine* **2014**, *9*, 773.
[31] G. Ciofani, L. Ricotti, S. Danti, S. Moscato, C. Nesti, D. D'Alessandro, D. Dinucci, F. Chiellini, A. Pietrabissa, M. Petrini, *Int. J. Nanomed.* **2010**, *5*, 285.
[32] G. Ciofani, V. Raffa, A. Menciassi, A. Cuschieri, *Biotechnol. Bioeng.* **2008**, *101*, 850.
[33] G. Ciofani, S. Danti, D. D'Alessandro, L. Ricotti, S. Moscato, G. Bertoni, A. Falqui, S. Berrettini, M. Petrini, V. Mattoli, A. Menciassi, *ACS Nano* **2010**, *4*, 6267.
[34] G. Ciofani, S. Danti, D. D'Alessandro, S. Moscato, A. Menciassi, *Biochem. Biophys. Res. Commun.* **2010**, *394*, 405.

[35] M. B. Jakubinek, K. S. Kim, C. Homenick, O. Kodra, S. Walker, B. Simard, *Can. J. Chem.* **2019**, *97*, 457.
[36] T. Stoeger, C. Reinhard, S. Takenaka, A. Schroeppel, E. Karg, B. Ritter, J. Heyder, H. Schulz, *Environ. Health Perspect.* **2006**, *114*, 328.
[37] T. M. Sager, C. Kommineni, V. Castranova, *Part. Fibre Toxicol.* **2008**, *5*, 17.
[38] G. Oberdörster, V. Castranova, B. Asgharian, P. Sayre, *J. Toxicol. Environ. Health, Part B* **2015**, *18*, 121.
[39] V. Kodali, B. D. Thrall, in *Studies on Experimental Toxicology and Pharmacology*, (Eds: M. S. Roberts, P. J. Kehrer, L.-O. Klotz), Springer International Publishing, Cham **2015**, pp. 347–367.
[40] H. Zhang, Z. Ji, T. Xia, H. Meng, C. Low-Kam, R. Liu, S. Pokhrel, S. Lin, X. Wang, Y.-P. Liao, M. Wang, L. Li, R. Rallo, R. Damoiseaux, D. Telesca, L. Mädler, Y. Cohen, J. I. Zink, A. E. Nel, *ACS Nano* **2012**, *6*, 4349.
[41] W. J. G. M. Peijnenburg, E. Ruggiero, M. Boyles, F. Murphy, V. Stone, D. A. Elam, K. Werle, W. Wohlleben, *Materials* **2020**, *13*, 2235.
[42] A. Manke, L. Wang, Y. Rojanasakul, *Biomed Res. Int.* **2013**, *2013*, 942916.
[43] C. Ge, Y. Li, J.-J. Yin, Y. Liu, L. Wang, Y. Zhao, C. Chen, *NPG Asia Mater.* **2012**, *4*, e32.
[44] I. Fenoglio, G. Greco, M. Tomatis, J. Muller, E. Raymundo-Piñero, F. Béguin, A. Fonseca, J. B. Nagy, D. Lison, B. Fubini, *Chem. Res. Toxicol.* **2008**, *21*, 1690.
[45] V. E. Kagan, Y. Y. Tyurina, V. A. Tyurin, N. V. Konduru, A. I. Potapovich, A. N. Osipov, E. R. Kisin, D. Schwegler-Berry, R. Mercer, V. Castranova, A. A. Shvedova, *Toxicol. Lett.* **2006**, *165*, 88.
[46] A. Bahl, B. Hellack, M. Wiemann, A. Giusti, K. Werle, A. Haase, W. Wohlleben, *NanoImpact* **2020**, *19*, 100234.
[47] T. Taniguchi, K. Kimoto, M. Tansho, S. Horiuchi, S. Yamaoka, *Chem. Mater.* **2003**, *15*, 2744.
[48] Y. Lei, S. Pakhira, K. Fujisawa, H. Liu, C. Guerrero-Bermea, T. Zhang, A. Dasgupta, L. M. Martinez, S. R. Singamaneni, K. Wang, J. Shallenberger, A. L. Elías, R. Cruz-Silva, M. Endo, J. L. Mendoza-Cortes, M. Terrones, *Mater. Today* **2021**, *51*, 108.
[49] H. Jin, Y. Li, X. Li, Z. Shi, H. Xia, Z. Xu, G. Qiao, *Mater. Lett.* **2016**, *175*, 244.
[50] S.-H. Lee, M. J. Kim, S. Ahn, B. Koh, *Int. J. Mol. Sci.* **2020**, *21*, 1529.
[51] F. Murtagh, P. Legendre, *J Classif* **2014**, *31*, 274.
[52] G. Vietti, D. Lison, S. van den Brule, *Part. Fibre Toxicol.* **2016**, *13*, 11.
[53] M. Sayan, B. T. Mossman, *Part. Fibre Toxicol.* **2016**, *13*, 51.
[54] A. Haghani, R. Johnson, N. Safi, H. Zhang, M. Thorwald, A. Mousavi, N. C. Woodward, F. Shirmohammadi, V. Coussa, J. P. Wise, H. J. Forman, C. Sioutas, H. Allayee, T. E. Morgan, C. E. Finch, *Environ Int* **2020**, *136*, 105510.
[55] H. Lin, Z. Song, A. Bianco, *J Environ Sci Health C Environ Carcinog Ecotoxicol Rev* **2021**, *56*, 333.
[56] Y. M. Janssen, A. Barchowsky, M. Treadwell, K. E. Driscoll, B. T. Mossman, *Proc. Natl. Acad. Sci. U. S. A.* **1995**, *92*, 8458.
[57] K. E. Zychowski, V. Kodali, M. Harmon, C. R. Tyler, B. Sanchez, Y. O. Suarez, G. Herbert, A. Wheeler, S. Avasarala, J. M. Cerrato, N. K. Kunda, P. Muttil, C. Shuey, A. Brearley, A.-M. Ali, Y. Lin, M. Shoeb, A. Erdely, M. J. Campen, *Toxicol. Sci.* **2018**, *164*, 101.
[58] P. J. Barnes, M. Karin, *N. Engl. J. Med.* **1997**, *336*, 1066.
[59] T. Liu, L. Zhang, D. Joo, S.-C. Sun, *Signal Transduct Target Ther* **2017**, *2*, 17023.
[60] N. Majumder, M. Velayutham, D. Bitounis, V. K. Kodali, M. H. H. Mazumder, J. Amedro, V. V. Khramtsov, A. Erdely, T. Nurkiewicz, P. Demokritou, E. E. Kelley, S. Hussain, *Redox Biol.* **2021**, *47*, 102161.
[61] V. Castranova, D. Porter, L. Millecchia, J. Y. C. Ma, A. F. Hubbs, A. Teass, in *Oxygen/Nitrogen Radicals: Cell Injury and Disease* (Eds: V. Vallyathan, X. Shi, V. Castranova), Springer, Boston **2002**, pp. 177–184.
[62] R. Simón-Vázquez, T. Lozano-Fernández, A. Dávila-Grana, A. González-Fernández, *Int. J. Nanomed.* **2016**, *11*, 4657.
[63] A. R. Murray, E. Kisin, S. S. Leonard, S. H. Young, C. Kommineni, V. E. Kagan, V. Castranova, A. A. Shvedova, *Toxicology* **2009**, *257*, 161.
[64] X. He, S.-H. Young, D. Schwegler-Berry, W. P. Chisholm, J. E. Fernback, Q. Ma, *Chem. Res. Toxicol.* **2011**, *24*, 2237.
[65] J. Dong, Q. Ma, *Front Pharmacol* **2019**, *10*, 1140.
[66] V. Hornung, F. Bauernfeind, A. Halle, E. O. Samstad, H. Kono, K. L. Rock, K. A. Fitzgerald, E. Latz, *Nat. Immunol.* **2008**, *9*, 847.
[67] J. Palomäki, E. Välimäki, J. Sund, M. Vippola, P. A. Clausen, K. A. Jensen, K. Savolainen, S. Matikainen, H. Alenius, *ACS Nano* **2011**, *5*, 6861.
[68] J. M. Hillegass, J. M. Miller, M. B. MacPherson, C. M. Westbom, M. Sayan, J. K. Thompson, S. L. Macura, T. N. Perkins, S. L. Beuschel, V. Alexeeva, H. I. Pass, C. Steele, B. T. Mossman, A. Shukla, *Part. Fibre Toxicol.* **2013**, *10*, 39.
[69] B. Sun, X. Wang, Z. Ji, R. Li, T. Xia, *Small* **2013**, *9*, 1595.
[70] S. W. Marvel, K. To, F. A. Grimm, F. A. Wright, I. Rusyn, D. M. Reif, *BMC Bioinformatics* **2018**, *19*, 80.
[71] M. G. Dorrington, I. D. C. Fraser, *Front Immunol* **2019**, *10*, 705.
[72] T. Xia, R. F. Hamilton Jr., J. C. Bonner, E. D. Crandall, A. Elder, F. Fazlollahi, T. A. Girtsman, K. Kim, S. Mitra, S. A. Ntim, *Environ Health Perspect* **2013**, *121*, 683.
[73] G. Zito, M. Buscetta, M. Cimino, P. Dino, F. Bucchieri, C. Cipollina, *Int. J. Mol. Sci.* **2020**, *21*, 4294.
[74] J. Schwartz, *Environ. Res.* **1994**, *64*, 26.
[75] D. W. Dockery, C. A. Pope, X. Xu, J. D. Spengler, J. H. Ware, M. E. Fay, B. G. Ferris, F. E. Speizer, *N. Engl. J. Med.* **1993**, *329*, 1753.
[76] B. Neupane, M. Jerrett, R. T. Burnett, T. Marrie, A. Arain, M. Loeb, *Am J. Respir. Crit. Care Med.* **2010**, *181*, 47.
[77] B. D. Thrall, V. Kodali, S. Skerrett, D. G. Thomas, C. W. Frevert, J. G. Pounds, J. G. Teeguarden, *NanoImpact* **2019**, *14*, 100155.
[78] G. DeLoid, B. Casella, S. Pirela, R. Filoramo, G. Pyrgiotakis, P. Demokritou, L. Kobzik, *NanoImpact* **2016**, *2*, 70.
[79] V. Kodali, M. H. Littke, S. C. Tilton, J. G. Teeguarden, L. Shi, C. W. Frevert, W. Wang, J. G. Pounds, B. D. Thrall, *ACS Nano* **2013**, *7*, 130709111523004.
[80] A. A. Shvedova, J. P. Fabisiak, E. R. Kisin, A. R. Murray, J. R. Roberts, Y. Y. Tyurina, J. M. Antonini, W. H. Feng, C. Kommineni, J. Reynolds, A. Barchowsky, V. Castranova, V. E. Kagan, *Am. J. Respir. Cell Mol. Biol.* **2008**, *38*, 579.
[81] L. M. Falcone, A. Erdely, R. Salmen, M. Keane, L. Battelli, V. Kodali, L. Bowers, A. B. Stefaniak, M. L. Kashon, J. M. Antonini, P. C. Zeidler-Erdely, *PLoS One* **2018**, *13*, e0209413.
[82] J. M. Antonini, H. M. Yang, J. Y. Ma, J. R. Roberts, M. W. Barger, L. Butterworth, T. G. Charron, V. Castranova, *Inhal Toxicol* **2000**, *12*, 1017.
[83] J. M. Antonini, J. R. Roberts, M. R. Jernigan, H.-M. Yang, J. Y. C. Ma, R. W. Clarke, *Toxicol. Sci.* **2002**, *70*, 110.
[84] J. H. Shannahan, W. Bai, J. M. Brown, *Recept. Clin. Invest.* **2015**, *2*, e811.
[85] Y. Suzuki, S. Tada-Oikawa, G. Ichihara, M. Yabata, K. Izuoka, M. Suzuki, K. Sakai, S. Ichihara, *Toxicol. Appl. Pharmacol.* **2014**, *278*, 16.
[86] ASTM, in *ASTM B922-20*, ASTM International, West Conshohocken, PA **2020**.
[87] D. Porter, K. Sriram, M. Wolfarth, A. Jefferson, D. Schwegler-Berry, M. E. Andrew, V. Castranova, *Nanotoxicology* **2008**, *2*, 144.
[88] K. Fraser, V. Kodali, N. Yanamala, M. E. Birch, L. Cena, G. Casuccio, K. Bunker, T. L. Lersch, D. E. Evans, A. Stefaniak, M. A. Hammer, M. L. Kashon, T. Boots, T. Eye, J. Hubczak, S. A. Friend, M. Dahm, M. K. Schubauer-Berigan, K. Siegrist, D. Lowry, A. K. Bauer, L. M. Sargent, A. Erdely, *Part. Fibre Toxicol.* **2020**, *17*, 62.
[89] J. R. Roberts, R. R. Mercer, A. B. Stefaniak, M. S. Seehra, U. K. Geddam, I. S. Chaudhuri, A. Kyrlidis, V. K. Kodali, T. Sager, A. Kenyon, S. A. Bilgesu, T. Eye, J. F. Scabilloni, S. S. Leonard,

N. R. Fix, D. Schwegler-Berry, B. Y. Farris, M. G. Wolfarth, D. W. Porter, V. Castranova, A. Erdely, *Part. Fibre Toxicol.* **2016**, *13*, 34.
[90] EPA, Benchmark Dose Software (BMDS), United States Environmental Protection Agency, https://www.epa.gov/bmds (accessed: February 2022).
[91] S. S. Leonard, J. R. Roberts, J. M. Antonini, V. Castranova, X. Shi, *Mol. Cell. Biochem.* **2004**, *255*, 171.
[92] A. B. Stefaniak, C. J. Harvey, V. C. Bukowski, S. S. Leonard, *J Occup Environ Hyg* **2009**, *7*, 23.
[93] B. Halliwell, J. M. Gutteridge, *Free Radicals in Biology and Medicine*, Oxford University Press, New York **2015**.
[94] J. H. WardJr., M. E. Hook, *Educ. Psychol. Meas.* **1963**, *23*, 69.